iScience

CellPress

Article

Variable Assembly of EMRE and MCU Creates Functional Channels with Distinct Gatekeeping Profiles

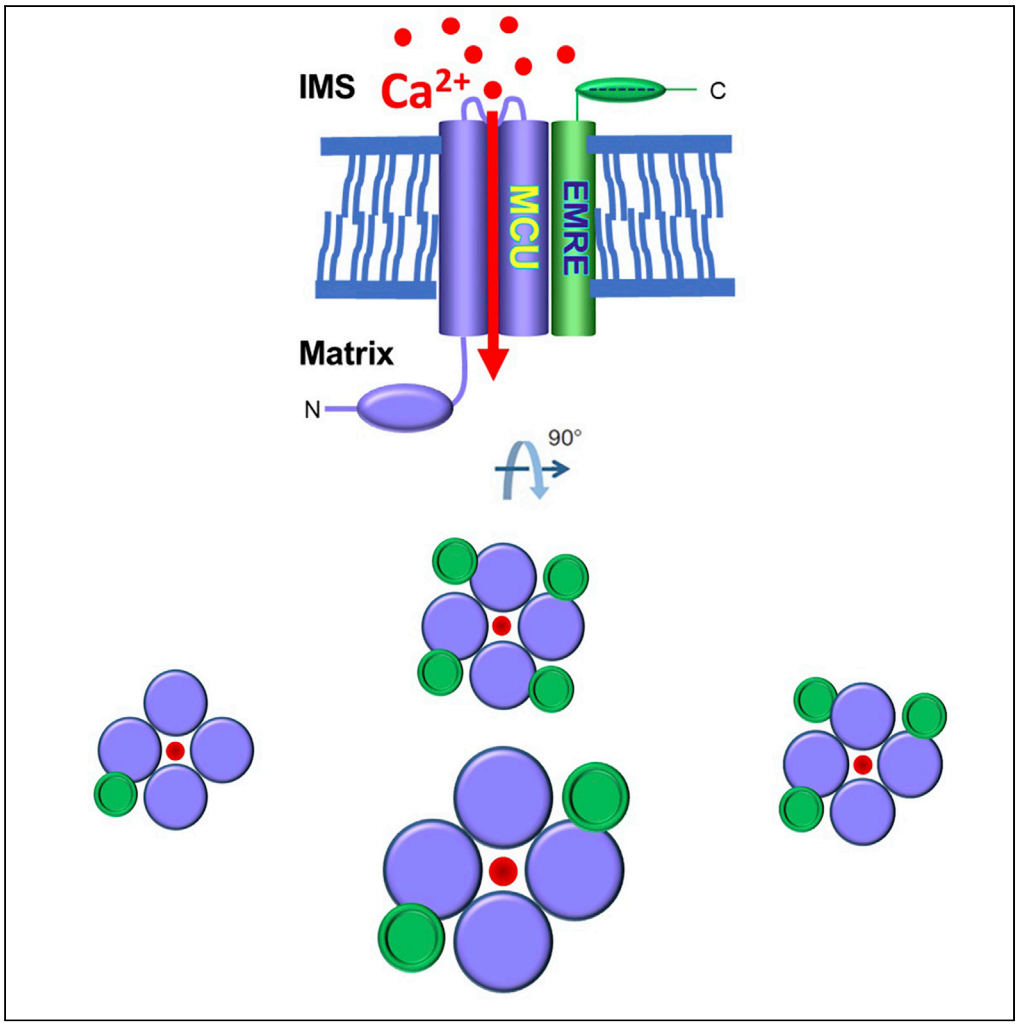

Riley Payne, Carmen Li, J. Kevin Foskett

foskett@pennmedicine.upenn.edu

HIGHLIGHTS

Mitochondrial Ca^{2+} uptake is mediated by the MCU Ca^{2+} ion channel

EMRE is required for MCU activity and for MCU interactions with MICU proteins

The EMRE:MCU stoichiometry of an MCU channel *in vivo* is unknown

MCU does not require four EMRE, with most endogenous channels containing two

Payne et al., iScience *23*, 101037
April 24, 2020
https://doi.org/10.1016/j.isci.2020.101037

iScience

CellPress

Article

Variable Assembly of EMRE and MCU Creates Functional Channels with Distinct Gatekeeping Profiles

Riley Payne,[1] Carmen Li,[1] and J. Kevin Foskett[1,2,3,*]

SUMMARY

MCU is a Ca^{2+}-selective channel that mediates mitochondrial Ca^{2+} influx. The human channel contains tetrameric pore-forming MCU, regulatory subunits MICU1/2, and EMRE that is required both for channel function and MICU1/2-mediated Ca^{2+} regulation. A structure of MCU with EMRE revealed a 4:4 stoichiometry, but the stoichiometry *in vivo* is unknown. Expression of tagged EMRE and MCU at a 1:10 ratio in cells lacking EMRE and MCU restored channel activity but not full channel gatekeeping. Increasing EMRE expression enhanced gatekeeping, raising the cytoplasmic Ca^{2+} concentration ($[Ca^{2+}]_c$) threshold for channel activation. MCU-EMRE concatemers creating channels with 1EMRE:4MCU restored Ca^{2+} uptake in cells, whereas cells expressing concatemers that enforced a 4EMRE:4MCU stoichiometry demonstrated enhanced channel gatekeeping. Concatemers enforcing 2EMRE/4MCU recapitulated the activity, gatekeeping, and size of endogenous channels. Thus, MCU does not require four EMRE, with most endogenous channels containing two, but complexes with 1–4 EMRE have activity with full or partial gatekeeping.

INTRODUCTION

Ca^{2+} uptake by energized mitochondria regulates bioenergetics, apoptosis, and global Ca^{2+} signaling. The primary pathway for mitochondrial Ca^{2+} uptake is the mitochondrial calcium uniporter (MCU), a Ca^{2+}-selective ion channel in the inner mitochondrial membrane (IMM) (Kirichok et al., 2004). MCU-mediated Ca^{2+} uptake is driven by the large negative IMM potential ($\Delta\Psi_m$) generated by proton pumping into the intermembrane space (IMS) by the electron transport chain. Despite the large thermodynamic driving force, mitochondrial Ca^{2+} uptake is tightly regulated to maintain low matrix $[Ca^{2+}]$ ($[Ca^{2+}]_m$) and prevent opening of the permeability transition pore, $\Delta\Psi_m$ depolarization, and cell death, while meeting dynamic energy demands of the cell. The MCU channel exists as a protein complex that (in metazoans) comprises several proteins: MCU contains two transmembrane helices (TM1 and TM2) and comprises the channel pore-forming subunit (Baughman et al., 2011) (De Stefani et al., 2011); MICU1 and its paralogs MICU2 and MICU3 are IMS-localized elements that sense cytoplasmic $[Ca^{2+}]$ ($[Ca^{2+}]_c$) to regulate channel activity (Perocchi et al., 2010) (Mallilankaraman et al., 2012) (Plovanich et al., 2013) (Csordás et al., 2013) (Kamer and Mootha, 2014) (Patron et al., 2014) (Payne et al., 2017); and EMRE is a single-pass transmembrane protein that both is essential for MCU channel activity (Sancak et al., 2013) (Kovács-Bogdán et al., 2014) (Yamamoto et al., 2016) and helps tether MICU proteins to the channel complex (Tsai et al., 2016). Although expression of each of these subunits is necessary for proper channel permeation, gating, and regulation, their stoichiometry in the functional MCU complex is largely unknown.

Although originally the pore was believed to assemble as a pentamer (Oxenoid et al., 2016), recent crystal- and cryo-EM structures of full-length fungal and metazoan MCU channels revealed that the pore assembles as a homo-tetramer, in which the transmembrane domains adopt a 4-fold symmetry that stabilizes the selectivity filter (Baradaran et al., 2018) (Yoo et al., 2018) (Wang et al., 2019) (Fan et al., 2018) (Nguyen et al., 2018). MICU1 forms homo-dimers as well hetero-dimers with its paralogs MICU2 (Patron et al., 2014) (Petrungaro et al., 2015) and MICU3 (Patron et al., 2019). MICU1 homo-dimers inhibit MCU channel activity at low (<500 nM) $[Ca^{2+}]_c$, a process referred to as "gatekeeping." They also contribute to cooperative activation of Ca^{2+} uptake when this threshold is exceeded by Ca^{2+} binding to its two EF-hand domains (Mallilankaraman et al., 2012) (Csordás et al., 2013) (Hoffman et al., 2013) (Patron et al., 2014) (Kamer and Mootha, 2014) (Wang et al., 2014) (Antony et al., 2016) (Liu et al., 2016) (Payne et al., 2017). MICU2 requires MICU1 to stabilize its expression and exists as an obligate hetero-dimer with MICU1 (Plovanich et al., 2013) (Patron et al., 2014) (Payne et al., 2017). MICU2 tunes the $[Ca^{2+}]_c$ threshold for relief of MICU1-

[1]Department of Physiology, Perelman School of Medicine, University of Pennsylvania, Philadelphia, PA 19104, USA

[2]Department of Cell and Developmental Biology, Perelman School of Medicine, University of Pennsylvania, Philadelphia, PA 19104, USA

[3]Lead Contact

*Correspondence: foskett@pennmedicine.upenn.edu

https://doi.org/10.1016/j.isci.2020.101037

mediated gatekeeping and the gain of cooperative Ca^{2+} activation of MCU open probability, mediated by Ca^{2+} binding to its EF hands that have different affinities from those in MICU1 (Kamer et al., 2017) (Payne et al., 2017). MICU1 and MICU2 are broadly expressed, whereas MICU3 is found exclusively in the central nervous system and appears to be structurally and functionally similar to MICU2 (Plovanich et al., 2013) (Patron et al., 2019) (Xing et al., 2019). MCU is likely regulated primarily by MICU1/2 dimers in most cells (Patron et al., 2014) (Payne et al., 2017). It has been suggested that MICU1 associates with the channel complex in part by a direct interaction with MCU by an electrostatic mechanism involving positively charged residues in MICU1 and negatively charged residues associated with the pore domain of MCU (Paillard et al., 2018) (Phillips et al., 2019). MICU2 lacks analogous basic residues, consistent with the fact that MICU2 requires dimerization with MICU1 for its association with the complex. The number of MICU1/2 dimers that associate with one MCU channel is unknown.

MICU1/2 association with the channel is also mediated by interactions with EMRE. A conserved polyacidic C terminus of EMRE faces into the IMS where it interacts with a polybasic region in the N terminus of MICU1 (but not MICU2) (Sancak et al., 2013) (Hoffman et al., 2013) (Yamamoto et al., 2016) (Tsai et al., 2016) (Vais et al., 2016). This interaction is required for the gatekeeping function of MICU1/2 since deletion of the polyacidic region or neutralization of its charge abolishes normal gatekeeping, causing mitochondrial Ca^{2+} overload (Tsai et al., 2016) (Vais et al., 2016). In addition, binding of EMRE to MCU is necessary for channel activity. In the absence of EMRE, MCU is expressed normally but it lacks function. The association of EMRE with the channel complex is mediated by transmembrane interactions with MCU (Tsai et al., 2016). A recent cryo-electron microscopy structure of human MCU channel in complex with EMRE (Wang et al., 2019) revealed a 4 EMRE:4 MCU stoichiometry, mediated largely by hydrophobic interactions between the transmembrane domain (TMD) of EMRE and TM1 in MCU. The structure revealed an asymmetric distribution of MCU N-terminal domains (NTDs) among subunits, in contrast to a dimer-of-NTD-dimers observed in fungal MCU channels (Baradaran et al., 2018) (Yoo et al., 2018) (Wang et al., 2019) (Lee et al., 2016). In addition, dimerization between NTDs of two assembled human MCU tetramers suggested that metazoan MCU channels may form dimers *in situ*.

An important question is whether this cryo-EM MCU-EMRE structure recapitulates the stoichiometry of MCU and EMRE in the functional channel complex *in vivo*. Furthermore, it is unknown whether the same or different numbers of EMRE subunits are required for MCU activity on the one hand and normal MICU1/2-mediated gatekeeping and cooperative activation on the other. EMRE (but not MCU) is rapidly turned over by degradation through the activity of IMM-associated matrix-AAA (mAAA) proteases (Tsai et al., 2017) (König et al., 2016). Such rapid turnover could result in variable relative steady-state expression levels of EMRE and MCU that could alter the stoichiometry in cells. If MCU requires four EMRE for its activity, then absence of a single EMRE subunit from the complex would lead to complete loss of channel activity. On the other hand, if fewer than four EMRE subunits per MCU tetramer are sufficient for activity but fail to properly tether MICU1/2 dimers to the complex, such channels may be functional but exhibit altered gatekeeping and cooperative-activation profiles.

We have addressed these questions by determining the consequences of altering the number of EMRE subunits in each complex on both channel activity and regulation by MICU1/2. First, we manipulated the relative MCU and EMRE expression ratios in cells and correlated them with functional features. Second, we created a series of MCU-EMRE concatemers with multiple concatenated MCU subunits fused to EMRE in order to "fix" their stoichiometries in each channel complex. These approaches enabled functional and biochemical comparison of channels with a range of EMRE:MCU stoichiometries to endogenous channel complexes. Our results suggest that an MCU channel largely exists in association with fewer than four and more than one EMRE subunit, likely two.

RESULTS

Expression of EMRE and MCU in Double-KO Cells Restores Channel Activity but Not Gatekeeping

To create cells in which relative MCU and EMRE protein expression levels could be directly measured and correlated with functional outcomes, we first created a cell line in which all genomic copies of both *MCU* and *EMRE* were inactivated. This was accomplished by CRISPR/Cas9-mediated genetic knockout (KO) of *MCU* in HEK293T cells in which all *EMRE* genes had already been inactivated (provided by V. Mootha), hereafter referred to as MEKO cells. Inactivating mutations in the *EMRE* and *MCU* genes were verified

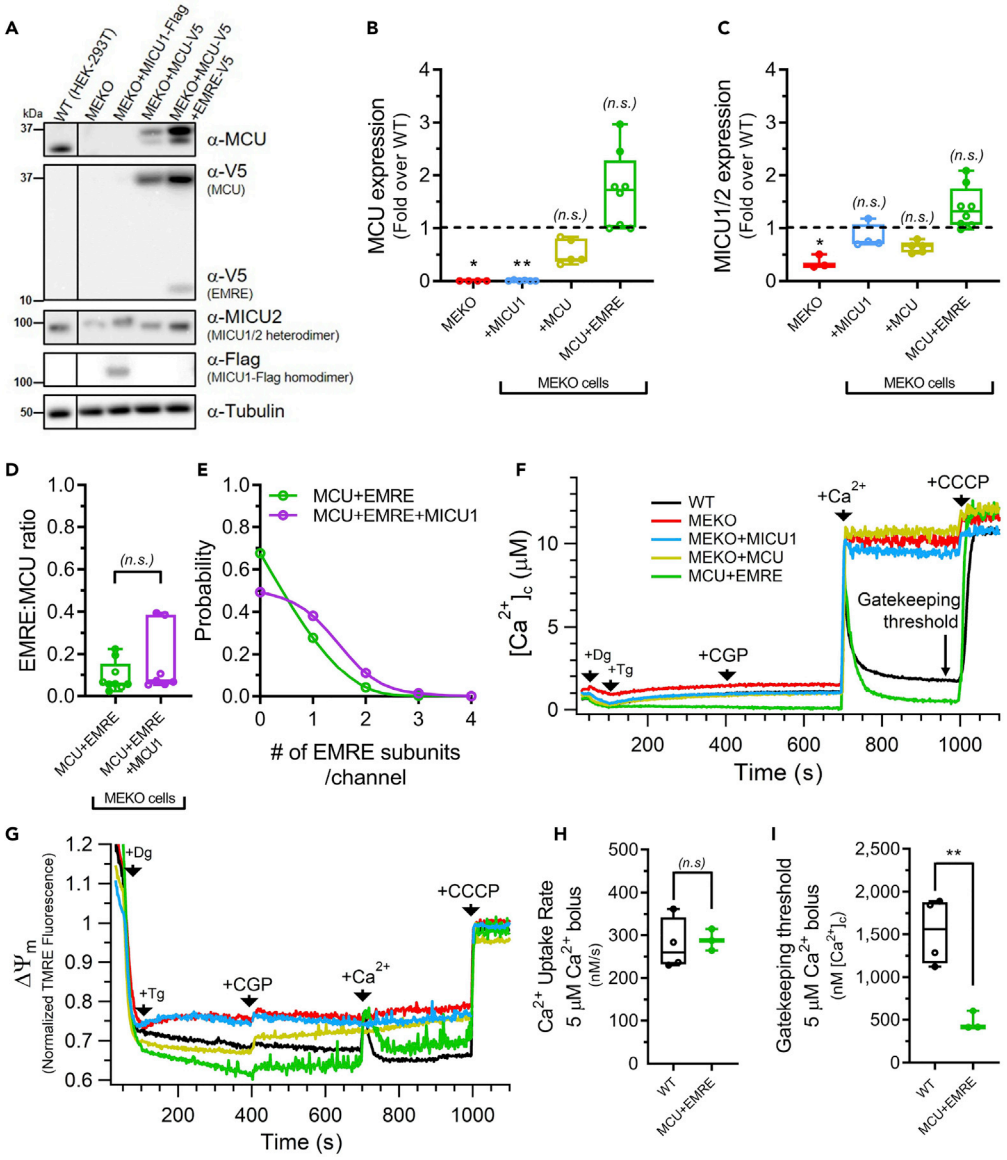

Figure 1. Expression of EMRE and MCU in Double-KO Cells Restores Channel Activity but Not Gatekeeping

(A) Western blots of MCU, V5-tag, MICU2, FLAG tag, and β-tubulin from whole-cell lysates of WT (HEK293T) cells, or MCU/EMRE KO (MEKO) cells +/− stable expression of MICU1-FLAG, MCU-V5, or MCU-V5 and EMRE-V5. Two bands for MCU-V5 protein due to low-level degradation of V5-tag, with upper band representing full-length MCU-V5. MICU2- and FLAG-blots performed under non-reducing conditions, such that MICU2 bands represent MICU1/2 hetero-dimers and FLAG bands represent MICU1-FLAG homo-dimers.

(B) Quantification of MCU western blot band intensity for cell lines in (A) from n ≥ 4 independent experiments. Mean pixel density corrected for β-tubulin intensity and normalized to endogenous MCU band intensity in WT cells for each experiment. Replicate measurements: hollow circles; boxes: 25th–75th percentile with line at median; error bars: range of all measurements. p Values: pairwise comparisons with WT cells (*p < 0.05; **p < 0.01; n.s., not different; Dunnett's multiple comparisons test).

(C) MICU2 western blot band intensity for cell lines in (A) from n ≥ 4 independent experiments under non-reducing conditions, quantified as described in (B).

(D) EMRE:MCU expression ratio in MCU + EMRE and MCU + EMRE + MICU1 cells (n = 9 independent experiments). Ratio calculated by dividing mean pixel density of EMRE-V5 band by that of MCU-V5 band for each experiment. Replicate measurements: hollow circles; boxes: 25th–75th percentile with line at median; error bars: range of all measurements. EMRE:MCU expression ratio in MCU + EMRE cells is 0.09 ± 0.07 (mean ± SD).

Figure 1. *Continued*

(E) Probability distribution histogram of number of EMRE subunits per MCU channel in MCU + EMRE and MCU + EMRE + MICU1 cells based on mean EMRE:MCU expression ratio calculated in (D). Points: mean probability of obtaining 0–4 EMRE subunits per channel based on binomial distribution. Solid lines: spline fits of all data points. At this EMRE:MCU expression ratio, >98% of channels predicted to associate with 0, 1, or 2 EMRE subunits.

(F) Cytoplasmic (bath) $[Ca^{2+}]$ ($[Ca^{2+}]_c$) of cell lines in (A) measured with FuraFF (K_D = 5.5 μM). Cells treated with digitonin (Dg), thapsigargin (Tg), and CGP37157 (CGP) as indicated. Bolus addition of Ca^{2+} to raise $[Ca^{2+}]_c$ to 8–10 μM at t = 700 s to stimulate MCU Ca^{2+} uptake. 2 μM CCCP added at t = 1,000 s to uncouple $\Delta\Psi_m$ and release mitochondrial Ca^{2+} content. Representative traces from n ≥ 3 independent replicates for each cell line. Both MCU and EMRE required for Ca^{2+} uptake activity.

(G) Relative $\Delta\Psi_m$ for experiments shown in (F). Transient depolarization observed in response to Ca^{2+} uptake, whereas addition of CCCP collapsed $\Delta\Psi_m$.

(H) Ca^{2+}-uptake rates for WT and MCU + EMRE cells in response to bolus additions of $CaCl_2$ that increased $[Ca^{2+}]_c$ by ~5 μM, n ≥ 3 independent experiments. Replicate measurements: hollow circles; boxes: 25^{th}–75^{th} percentile with line at median; error bars: range of all measurements. p Values: pairwise comparison of MCU + EMRE with WT cells (n.s., not different; Welch's unpaired t test). Ca^{2+}-uptake rates not different between WT and MCU + EMRE cells.

(I) Gatekeeping threshold for cell lines in (H) measured 300 s after bolus addition of ~5 μM free Ca^{2+}. Each point (hollow circle) represents independent experiment (n ≥ 3 for each condition). p Values: comparison of MCU + EMRE with WT cells (**p < 0.01; n.s., not different; Welch's unpaired t test). Gatekeeping-threshold $[Ca^{2+}]_c$ after uptake in MCU + EMRE cells was reduced (~500 nM) compared with WT levels (1.5–2 μM).

See also Figure S1.

by genomic sequencing. Western blotting revealed a complete loss of MCU protein expression (Figures 1A and 1B: red). MICU2 dimerizes with MICU1 under non-reducing conditions but does not form homo-dimers when expressed in MICU1 KO cells (Payne et al., 2017). Thus, MICU2 bands at ~100 kDa observed in non-reducing western blots correspond to MICU1/2 hetero-dimers. MEKO cells exhibited reduced expression of MICU1/2 dimers relative to wild-type (WT) HEK293T cells (Figures 1A and 1C: red), which increased upon stable overexpression of MICU1-FLAG (MEKO + MICU1 cells) to levels equivalent to those in WT cells (Figures 1A and 1C: blue). Similarly, stable transfection of MEKO cells with MCU-V5 (MEKO + MCU cells) restored both MCU and MICU1/2 dimer expression to WT levels (Figures 1A–1C: yellow). We were able to express MCU-V5 at ~10-fold higher levels than endogenous levels, even in MCU-KO cells. Similarly, we were able to express EMRE-V5 at high levels in EMRE-KO cells. However, we found that, when we co-expressed both MCU and EMRE in MEKO cells, neither protein expressed as strongly. Importantly, we screened numerous clones for each line to select the ones that had expression levels closest to the endogenous ones. Stable expression of EMRE-V5 in MEKO + MCU cells (MCU + EMRE cells) did not change MCU or MICU1/2 dimer expression relative to WT cells. EMRE in these stable lines was fully processed to its mature form (Figure S1A). The lack of available antibodies specific to the processed form of endogenous EMRE prevented comparison of EMRE levels between WT and MCU-EMRE cells. Consequently, expression levels of MCU and MICU1/2 in MCU + EMRE cells were similar to those in WT cells, whereas we do not know if the relative expression of MCU to EMRE in MCU + EMRE cells was similar to that in WT cells. Notably, EMRE-V5 expression was ~10-fold lower than MCU-V5 expression in MCU + EMRE cells (Figures 1A and 1D). Given this EMRE:MCU ratio, binomial probability predicts that >98% of MCU tetramers would associate with zero, one, or two EMRE (Figure 1E).

To evaluate MCU function, we simultaneously measured MCU-mediated Ca^{2+} uptake and relative mitochondrial membrane potential ($\Delta\Psi_m$) in permeabilized cells as previously described using the cell-impermeant Ca^{2+}-indicator dye FuraFF (K_D = 5.5 μM) (Mallilankaraman et al., 2012) (Payne et al., 2017) and tetramethylrhodamine ethyl ester (TMRE), respectively (Payne et al., 2017). Digitonin (Dg) was added to a suspension of cells to permeabilize the plasma membrane but leave the IMM intact (Figure 1F: t = 50 s). Thapsigargin (Tg) was added to inhibit the sarco/endoplasmic reticular calcium ATPase (SERCA), preventing Ca^{2+} uptake into the ER and releasing the ER Ca^{2+} stores into the bath (Figure 1F: t = 100–400 s). CGP37157 (CGP), an inhibitor of mitochondrial Na^+/Ca^{2+}-antiporter (NCLX)-mediated Ca^{2+} efflux, was added to isolate MCU as the only pathway for transport of Ca^{2+} between mitochondria and cytoplasm (Figure 1F: t = 400–700 s). Upon reaching a steady-state $[Ca^{2+}]_c$, acute addition of a Ca^{2+} bolus to the bath (i.e., cytoplasm) immediately elevated $[Ca^{2+}]_c$ to 8–10 μM, which was followed by clearance of Ca^{2+} in WT cells that reduced $[Ca^{2+}]_c$ to a steady-state level between 1 and 2 μM (Figure 1F: t = 700–1,000 s; black trace). A transient increase in TMRE fluorescence was observed (Figure 1G) as Ca^{2+} influx depolarized $\Delta\Psi_m$, which recovered as $[Ca^{2+}]_c$ approached a steady state due to closure of MCU. This steady state represents the $[Ca^{2+}]_c$ threshold at which uptake ceases, a hallmark of MICU1/2-mediated MCU gatekeeping. Finally,

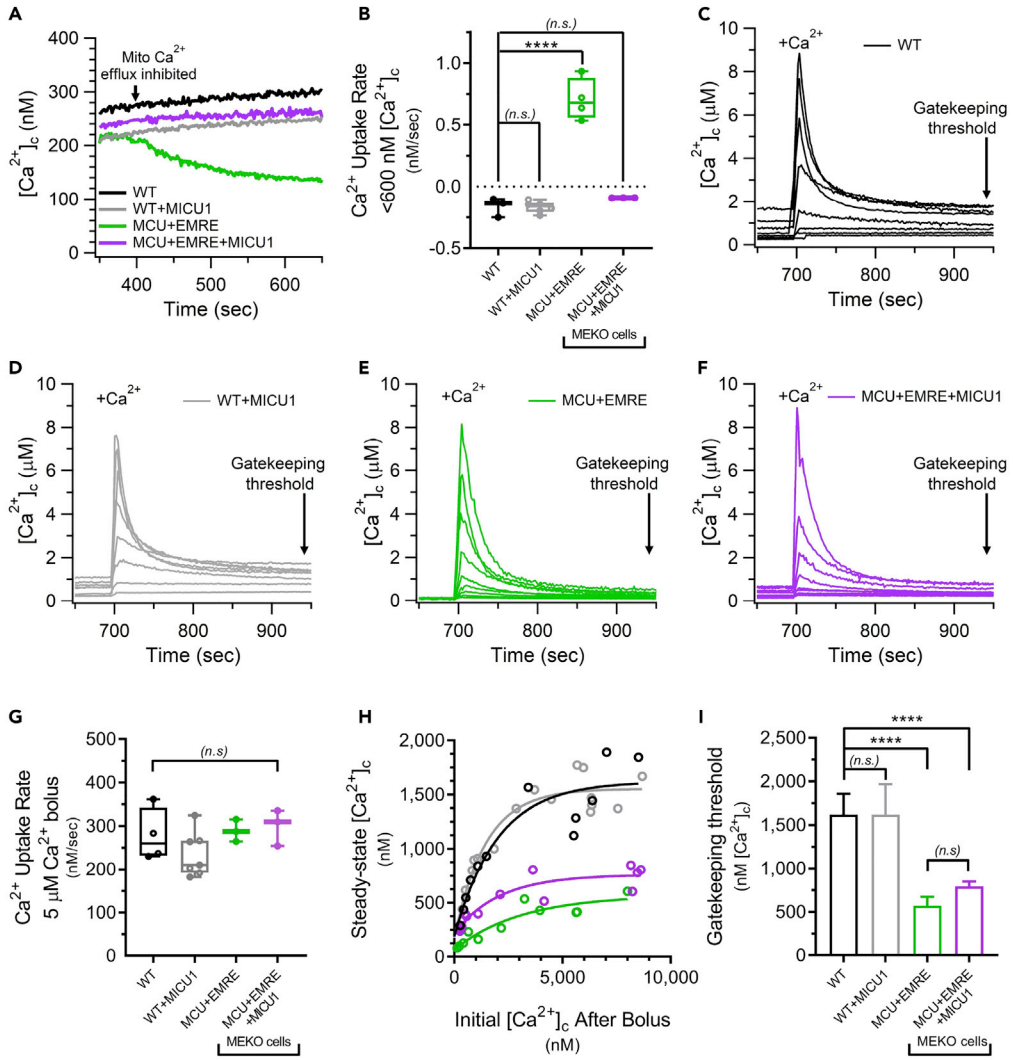

Figure 2. Overexpression of MICU1 Only Partially Restores Gatekeeping in MCU + EMRE Cells

(A) $[Ca^{2+}]_c$ responses to acute inhibition of NCLX-mediated Ca^{2+} efflux for WT (black), WT + MICU1 (gray), MCU + EMRE (green), and MCU + EMRE + MICU1 (purple) cells measured with high-affinity indicator Fura2. Representative traces from n ≥ 3 independent replicates for each cell line. Overexpression of MICU1-FLAG in MCU + EMRE cells rescued gatekeeping at low (<300 nM) $[Ca^{2+}]_c$.

(B) Ca^{2+}-uptake rate below 600 nM $[Ca^{2+}]_c$ in response to inhibition of NCLX-mediated Ca^{2+} efflux for cell lines in (A). Each point represents initial Ca^{2+}-uptake rate from an independent experiment (n ≥ 3 for each condition) determined by single-exponential fit to reduction of $[Ca^{2+}]_c$. Replicate measurements: hollow circles; boxes: 25th–75th percentile with line at median; error bars: range of all measurements. p Values: pairwise comparisons with WT cells ****p < 0.0001; n.s., not different; Tukey's multiple comparisons test).

(C–F) Ca^{2+} uptake, measured using the paradigm depicted in Figure 1F, in suspensions of permeabilized WT (C), WT + MICU1 (D), MCU + EMRE (E), and MCU + EMRE + MICU1 (F) cells in response to acute increases of $[Ca^{2+}]_c$ to between 0.1 and 10 μM. Representative traces from independent experiments with different bolus additions shown.

(G) Ca^{2+}-uptake rates for cell lines in (A) in response to bolus additions of $CaCl_2$ that increased $[Ca^{2+}]_c$ by ~5 μM from n ≥ 3 independent experiments. Replicate measurements: hollow circles; boxes: 25th–75th percentile with line at median; error bars: range of all measurements. p Values: pairwise comparison of each cell line with all other cell lines (n.s., not different; Tukey's multiple comparisons test). Ca^{2+}-uptake rates similar for all cell lines shown.

(H) Steady-state $[Ca^{2+}]_c$ for cell lines in (A) measured 300 s after bolus addition of 0.1–10 μM Ca^{2+} plotted as function of initial peak $[Ca^{2+}]_c$ after addition. Each point (hollow circle) represents an independent experiment (n ≥ 12 for each condition). Solid lines: one-phase association fits of steady-state $[Ca^{2+}]_c$ versus the initial $[Ca^{2+}]_c$ after addition.

Figure 2. *Continued*

(I) Comparison of gatekeeping-threshold $[Ca^{2+}]_c$ from non-linear fits in (H). Bars: mean of the plateau parameter for each fit ± SEM. p Values: comparison of each cell line with all other cell lines (****$p < 0.0001$; n.s., not different; Tukey's multiple comparisons test).

See also Figure S2.

the uncoupler carbonyl cyanide m-chlorophenyl hydrazone (CCCP) was added to dissipate $\Delta\Psi_m$ (Figure 1G), leading to a rapid increase in $[Ca^{2+}]_c$ as total mitochondrial matrix Ca^{2+} content was released (Figure 1F: t = 1,000–1,100 s). TMRE fluorescence in CCCP was used to determine the relative $\Delta\Psi_m$ between experiments.

Upon challenge with boluses of Ca^{2+} that increased $[Ca^{2+}]_c$ to ~10 μM, MEKO cells exhibited no reduction in $[Ca^{2+}]_c$ (Figure 1F: red trace) or change in $\Delta\Psi_m$ (Figure 1G: red trace), reflecting lack of mitochondrial Ca^{2+} uptake, as expected. MEKO + MICU1 cells (Figures 1F and 1G: blue traces) or MEKO + MCU cells (Figures 1F and 1G: yellow traces) also exhibited no MCU activity, because of the EMRE requirement for MCU channel activity (Sancak et al., 2013) (Kovács-Bogdán et al., 2014) (Yamamoto et al., 2016). In contrast, MCU + EMRE cells (Figures 1F–1H: green) exhibited mitochondrial Ca^{2+}-uptake rates and transient $\Delta\Psi_m$ depolarizations at $[Ca^{2+}]_c$ of 8–10 μM similar to WT cells (Figures 1F–1H: black). Surprisingly, the steady-state $[Ca^{2+}]_c$ achieved 200–300 s after uptake ceased was ~1.5–2 μM in WT cells (Figures 1F and 1I: black), whereas it was reduced to ~500 nM in MCU + EMRE cells (Figures 1F and 1I: green). Of note, reduction to levels lower than those achieved in WT cells is a feature of impaired gatekeeping (Mallilankaraman et al., 2012) (Csordás et al., 2013) (Kamer and Mootha, 2014) (Payne et al., 2017) (Patron et al., 2014) (Kamer et al., 2017). To explore this further, we measured MCU activity at low (100–600 nM) $[Ca^{2+}]_c$ using the high-affinity indicator Fura2 (K_D = 140 nM) following CGP addition. CGP was required because NCLX-mediated Ca^{2+} efflux can mask MCU-mediated influx even in the absence of full MICU1/2-mediated gatekeeping (Figures S1B and S1C: red traces). Acute CGP addition was without effect on $[Ca^{2+}]_c$ in WT cells (Figures 2A, 2B, and S1C: black) owing to MICU1/2 gatekeeping. A reduction in $[Ca^{2+}]_c$ following acute addition of CGP was observed in MICU1 KO cells, reflecting constitutive MCU activity (Figure S1C: red trace), as expected due to lack of gatekeeping (Mallilankaraman et al., 2012) (Csordás et al., 2013) (Kamer and Mootha, 2014) (Payne et al., 2017) (Patron et al., 2014). Notably, MCU + EMRE cells exhibited significant constitutive Ca^{2+} uptake (Figures 2A and 2B: green), confirming the lack of fully functional MICU1/2-mediated gatekeeping in these cells. MICU1/2 also mediates cooperative activation of MCU in response to higher $[Ca^{2+}]_c$ (Csordás et al., 2013) (Payne et al., 2017). Ca^{2+}-uptake rates in response to acute additions of Ca^{2+} between 0.1 and 10 μM (Figures 2C and 2E), plotted on a log/log scale, yielded a slope of ~2.8 in WT cells (Figure S1D: black), as previously observed (Payne et al., 2017). In contrast, the slope was ~1.6 in MCU + EMRE cells (Figure S1D: green). However, this apparent loss of cooperative activation was due solely to constitutive channel activity at low (<1–2 μM) $[Ca^{2+}]_c$ and not a loss of cooperative activation at higher $[Ca^{2+}]_c$ as seen in MICU1 KO cells. Thus, gatekeeping and cooperative activation of MCU were uncoupled in MCU + EMRE cells, a phenomenon not previously seen in cells lacking MICU1 and/or MICU2 expression (Csordás et al., 2013) (Payne et al., 2017).

Overexpression of MICU1 Only Partially Restores Gatekeeping in MCU + EMRE Cells

Although MICU1/2 dimer expression in MCU + EMRE cells was similar to that in WT cells (Figures 1A and 1C), we considered that, because of the low EMRE:MCU expression ratio in these cells (~1:10), gatekeeping was disturbed because most channels lacked enough EMRE to tether sufficient MICU1/2 dimers to the channels. Because MICU1 can directly associate with MCU (Paillard et al., 2018) (Phillips et al., 2019), we reasoned that over-expression of MICU1 in MCU-EMRE cells might restore gatekeeping despite low EMRE expression, by directly interacting with MCU. To test this, MICU1-FLAG was stably expressed in MCU + EMRE cells (MCU + EMRE + MICU1 cells) and in WT cells (WT + MICU1 cells). Expression of MCU (Figures S2A and S2B) and the EMRE:MCU expression ratio (Figure S2C; Figures 1D and 1E: purple) were similar in MCU + EMRE + MICU1 and MCU + EMRE cells. Only MICU1-FLAG homo-dimers were observed in non-reducing western blots of MICU1-overexpressing cells (Figure S2D), because of its high expression relative to MICU1 in WT cells (Figure S2E) as we previously showed using the same antibodies (Payne et al., 2017). Nevertheless, MICU1/2 dimer expression in MCU + EMRE + MICU1 cells (Figures S2F and S2G: purple) was not different from that of WT, although a small reduction was observed relative to MCU + EMRE cells (Figures S2F and S2G: green). In contrast, it was increased 2- to 3-fold in the WT + MICU1 cells compared with WT (Figures S2F and S2G: gray). We measured MCU activity at low (100–600 nM) $[Ca^{2+}]_c$ as described above. As expected, acute CGP addition was without effect on $[Ca^{2+}]_c$ in WT + MICU1 cells

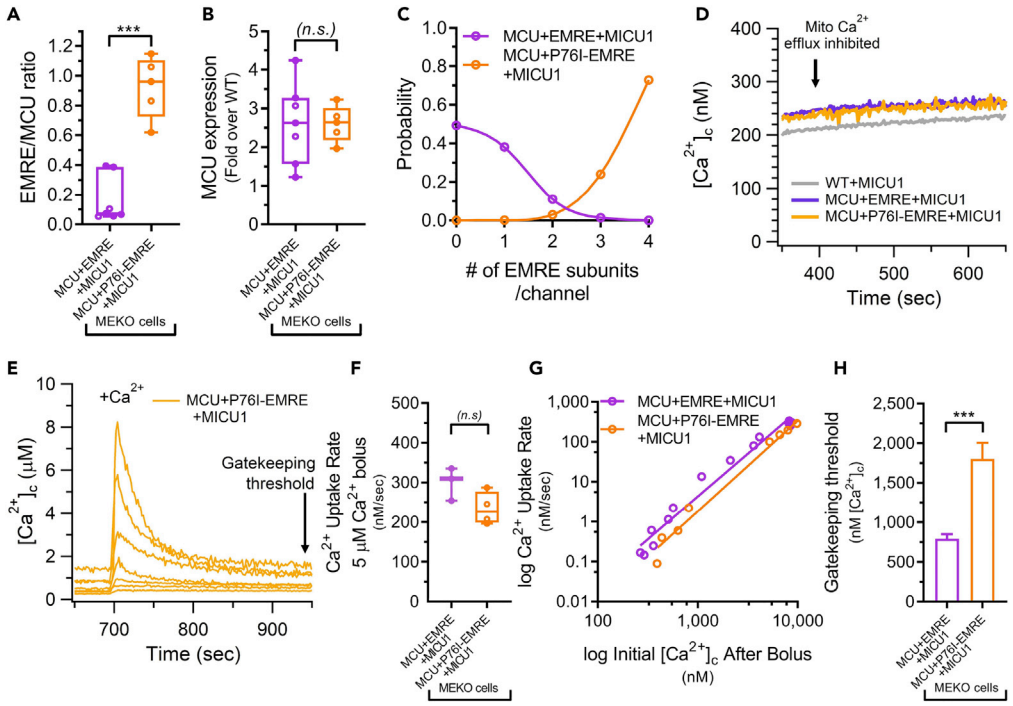

Figure 3. Increasing EMRE Expression Enhances MICU1/2-Mediated Gatekeeping

(A) EMRE:MCU expression ratio in whole-cell lysates of MCU + EMRE + MICU1 and MCU + P76I-EMRE + MICU1 cells from n ≥ 5 independent experiments. Ratio calculated by dividing mean pixel density of EMRE-V5 band by that of MCU-V5 band for each experiment. Replicate measurements: hollow circles; boxes: 25th–75th percentile with line at median; error bars: range of all measurements. p Value: comparison of MCU + EMRE + MICU1 cells with MCU + P76I-EMRE + MICU1 cells (***p < 0.001; unpaired t test with Welch's correction). EMRE:MCU expression ratio in MCU + P76I-EMRE + MICU1 cells is 0.92 ± 0.21 (mean ± SD).

(B) MCU western blot band intensity for cells in (A) from n ≥ 5 independent experiments. Mean pixel density corrected for β-tubulin intensity and normalized to endogenous MCU band intensity in WT cells for each experiment. Replicate measurements: hollow circles; boxes: 25th–75th percentile with line at median; error bars: range of all measurements. p Value: comparison of MCU + EMRE + MICU1 cells with MCU + P76I-EMRE + MICU1 cells (n.s., not different; unpaired t test with Welch's correction).

(C) Probability distribution histogram of expected number of EMRE per MCU channel in MCU + EMRE + MICU1 and MCU + P76I-EMRE + MICU1 cells based on EMRE:MCU expression ratios calculated in (A). Points represent mean probability of obtaining 0–4 EMRE subunits per channel based on binomial distribution. Solid lines: spline fits of all data points. EMRE:MCU expression ratio in MCU + P76I-EMRE + MICU1 cells predicts that >95% of MCU tetramers associate with three or four EMRE subunits.

(D) $[Ca^{2+}]_c$ response to acute inhibition of NCLX-mediated Ca^{2+} efflux for WT + MICU1 (gray), MCU + EMRE + MICU1 (purple), and MCU + P76I-EMRE + MICU1 (orange) cells measured with Fura2. Representative traces from n ≥ 3 independent replicates for each cell line.

(E) Ca^{2+} uptake in MCU + P76I-EMRE + MICU1 cells in response to acute increases of $[Ca^{2+}]_c$ to between 0.1 and 10 μM. Individual traces from independent experiments with series of bolus additions shown. Gatekeeping threshold in MCU + P76I-EMRE + MICU1 cells restored to WT levels.

(F) Ca^{2+}-uptake rates for MCU + EMRE + MICU1 (from Figure 2F) and MCU + P76I-EMRE + MICU1 cells in response to bolus additions of $CaCl_2$ that increased $[Ca^{2+}]_c$ by ~5 μM from n ≥ 3 independent experiments. Replicate measurements: hollow circles; boxes: 25th–75th percentile with line at median; error bars: range of all measurements. p Values: pairwise comparison of MCU + EMRE + MICU1 cells with MCU + P76I-EMRE + MICU1 cells (n.s., not different; unpaired t test with Welch's correction).

(G) Ca^{2+}-uptake rates between 0.1 and 10 μM $[Ca^{2+}]_c$ measured in (E) and Figure 2F plotted on $\log_{10}/\log_{10}$ scale. Each point (hollow circle) represents independent experiment. Solid lines: linear fits of ($\log_{10}$) Ca^{2+}-uptake rate versus ($\log_{10}$) $[Ca^{2+}]_c$. Slope of best-fit line, a measure of cooperativity of MCU activation, was similar between MCU + EMRE + MICU1 and MCU + P76I-EMRE + MICU1 cells.

(H) Comparison of gatekeeping-threshold $[Ca^{2+}]_c$ from non-linear fits (in Figure S3I). Bars represent mean of plateau parameter for each fit ±SEM. p Value: comparison of MCU + EMRE + MICU1 cells with MCU + P76I-EMRE + MICU1 cells

Figure 3. *Continued*

(***p < 0.001; n.s., not different; unpaired t test with Welch's correction). Gatekeeping threshold in MCU + P76I-EMRE + MICU1 was elevated relative to that in MCU + EMRE + MICU1 cells (from Figure 2F).

See also Figure S3.

(Figures 2A and 2B: gray) owing to MICU1/2 gatekeeping. MCU + EMRE cells exhibited significant constitutive Ca^{2+} uptake (Figures 2A and 2B: green), whereas gatekeeping at low $[Ca^{2+}]_c$ was restored in MCU + EMRE + MICU1 cells (Figures 2A and 2B: purple). This result suggests that gatekeeping can be reconstituted by EMRE-independent association of MICU1 with MCU. Ca^{2+}-uptake rates in response to Ca^{2+} boluses that elevated $[Ca^{2+}]_c$ by ~5 μM were not different between WT (Figures 2C and 2G: black), WT + MICU1 (Figures 2D and 2G: gray), MCU + EMRE (Figures 2E and 2G: green), and MCU + EMRE + MICU1 cells (Figures 2F and 2G: purple). There was an apparent increase in cooperative channel activation in MCU + EMRE + MICU1 cells (slope ~2.1) (Figure S2H: purple) relative to MCU + EMRE cells (slope ~1.6) (Figure S1D: green), but this could be attributed solely to the restoration of gatekeeping at low $[Ca^{2+}]_c$. Cooperativity of MCU activation was similar between the WT (Figure S1D: black) and WT + MICU1 (Figure S2H: gray) cells (slope ~2.8 for both). The normal threshold $[Ca^{2+}]_c$ for MCU activation was observed in WT and WT-MICU1 cells (~1.5 μM; Figures 2C and 2D; H-I: black versus gray), despite enhanced expression of MICU1 and 2. Importantly, however, the threshold in MCU + EMRE + MICU1 cells was ~800 nM (Figures 2F, 2H, and 2I: purple), still below that in WT cells. Thus, although MICU1 overexpression restored gatekeeping at low $[Ca^{2+}]_c$ in MCU + EMRE cells, presumably by directly interacting with MCU, it was insufficient to fully restore normal gatekeeping. We hypothesized that the low EMRE:MCU ratio in MCU + EMRE + MICU1 cells resulted in sub-stoichiometric association of EMRE with MCU that enabled channel gating but was insufficient to tether enough MICU1/2 dimers to reconstitute fully functional gatekeeping.

Increasing EMRE Expression Enhances MICU1/2-Mediated Gatekeeping

To test this, we increased the EMRE:MCU ratio by enhancing steady-state EMRE expression. Under normal conditions, mAAA proteases degrade EMRE (Tsai et al., 2017) (König et al., 2016). Substitution of a proline (P) residue with isoleucine (I) at amino acid position 76 in EMRE inhibits its degradation, increasing its expression without affecting channel function or gatekeeping (Tsai et al., 2017) (Figures S3A and S3B). We stably overexpressed C-terminal V5-tagged P76I-EMRE and MCU along with MICU1-FLAG (to ensure sufficient MICU1 to occupy all functional EMRE:MCU complexes) in the MEKO background (MCU + P76I-EMRE + MICU1 cells). EMRE expression was increased ~6-fold in MCU + P76I-EMRE + MICU1 cells compared with MCU + EMRE + MICU1 cells (Figure S3C; Figure 3A), whereas expression of MCU (Figures S3D and 3B) and MICU1/2 (Figures S3E and S3F) was similar between the two lines. Assuming random assembly of MCU/EMRE complexes, >95% of MCU tetramers are predicted to associate with three or four EMRE subunits in MCU + P76I-EMRE + MICU1 cells (Figure 3C: orange), in contrast to the one or two in the cells expressing WT EMRE (MCU + EMRE + MICU1 cells, Figure 3C: purple).

In the low-$[Ca^{2+}]_c$ regime, no differences in Ca^{2+} uptake were observed between WT + MICU1, MCU + EMRE + MICU1, and MCU + P76I-EMRE + MICU1 cells (Figure 3D), indicating that MICU1/2-mediated gatekeeping at low $[Ca^{2+}]_c$ was intact. In the higher-$[Ca^{2+}]_c$ regime (8–10 μM) (Figure 3E), the rates of Ca^{2+} uptake (Figure 3F) and cooperative activation (Figure 3G) were similar in MCU + EMRE + MICU1 and MCU + P76I-EMRE + MICU1 cells. Importantly, the steady-state $[Ca^{2+}]_c$ achieved after uptake (gatekeeping threshold) was significantly higher in the MCU + P76I-EMRE + MICU1 cells (~1.8 μM) than in MCU + EMRE + MICU1 cells (~800 nM) (Figures S3G and 3H). These results indicate that increasing the EMRE:MCU ratio elevates the $[Ca^{2+}]_c$ threshold required for relief of MICU1/2-mediated gatekeeping. Together, the data imply that MCU can associate with fewer than four EMRE per channel, which is sufficient to reconstitute channel activity and cooperative channel activation but may be insufficient to fully reconstitute MICU1/2-mediated channel gatekeeping. These results suggest that MCU activity can be differentially modulated by the number of EMRE subunits associated with the channel complex, possibly by determining the number of MICU1/2 dimers associated with it. Accordingly, a 4 EMRE:1 channel stoichiometry may not be fixed in cells.

MCU-EMRE Concatemers Form Channels with Fixed EMRE:MCU Stoichiometries

Co-expression of MCU and EMRE at known ratios cannot determine stoichiometries of the two proteins in the functional channel complex. To address this, we created a system in which we could establish fixed EMRE:MCU stoichiometries. We expressed a synthetic protein in which a truncated EMRE (ΔN30 a.a.) peptide

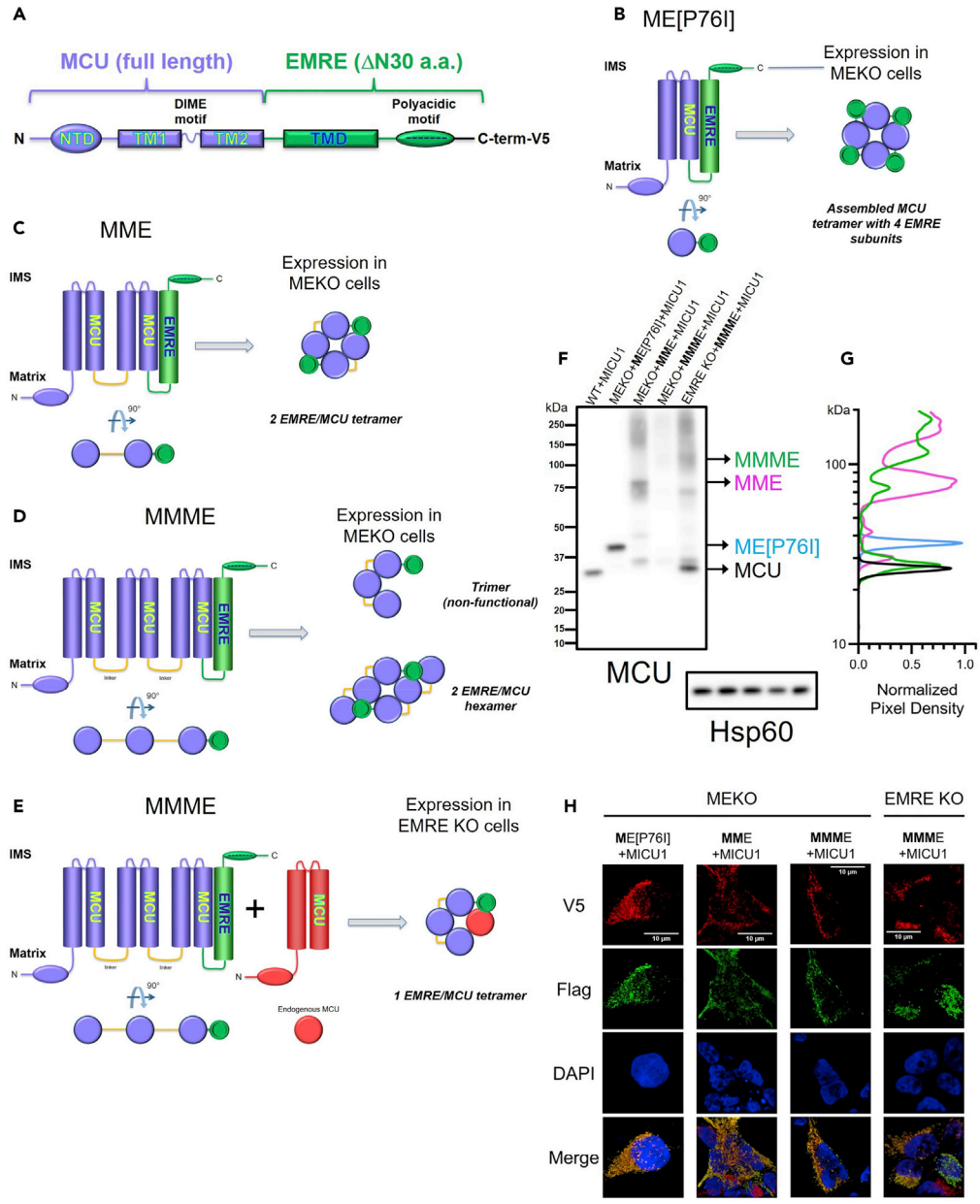

Figure 4. MCU-EMRE Concatemers Form Channels with Fixed EMRE:MCU Stoichiometries

(A) MCU-EMRE fusion protein comprised of full-length MCU fused to EMRE with the mitochondrial-targeting sequence truncated from its N terminus, followed by C-terminal V5 tag.

(B) Assembly of the ME concatemer (ME[P76I]) enforces a 1:1 EMRE:MCU stoichiometry in all channel complexes when expressed in MEKO cells.

(C) MME concatemer assembles as an MCU tetramer containing two EMRE subunits in MEKO cells.

(D) MMME concatemer cannot assemble as an MCU tetramer, but formation of hexamers or other higher-order oligomers may assemble as functional channels in MEKO cells.

(E) Expression of MMME in EMRE KO cells allows formation of channel complexes containing a single EMRE due to presence of endogenous MCU monomers.

(F) Western blot for MCU and Hsp60 in isolated mitochondria from representative clones of cell lines under reducing conditions.

(G) Quantification of molecular weight from normalized band intensity for α-MCU western blots in (F). Traces: mean of n = 3 replicate experiments. Single ~40-kDa band observed in cells expressing ME[P76I]; MME exhibited bands at ~80 and

Figure 4. *Continued*

160 kDa; MMME ran at ~110 and 220 kDa. Band at ~35 kDa in EMRE KO + MMME + MICU1 cells represents endogenous MCU.

(H) Immunofluorescence microscopy for V5 (MCU-EMRE concatemers), FLAG (MICU1), and DAPI in representative clones of cell lines in (F). All cell lines tested showed strong colocalization of both tags in mitochondria.

See also Figure S4.

containing a C-terminal V5 tag was fused to the C terminus of MCU (Figure 4A). This construct was previously shown to reconstitute MCU channel activity in the absence of endogenous MCU and EMRE (Tsai et al., 2016). We stably expressed the MCU-EMRE fusion protein (hereafter referred to as ME) in MEKO cells. Western blotting for V5 demonstrated that the fusion protein was expressed at the expected size, but probing with an α-MCU antibody also revealed a smaller band at the approximate molecular weight of MCU (Figure S4A). We surmised that this was caused by proteolytic cleavage. To minimize this degradation, we introduced the P76I mutation into the ME concatemer (ME[P76I]). Degradation observed in the original construct was mitigated by expression of the mutant construct (Figure S4A).

Expression of ME[P76I] in MEKO cells is predicted to result in a 1:1 EMRE:MCU stoichiometry in all channel complexes (Figure 4B). We also created MCU-EMRE[P76I] fusion proteins with two, three, or four concatenated MCU subunits fused to P76I-EMRE (hereafter referred to as MME, MMME, and MMMME, respectively). MME is predicted to dimerize, forming complexes with two EMRE subunits/MCU channel (Figure 4C), and MMMME is predicted to form complexes with one EMRE subunit/MCU tetramer. In contrast, MMME should be unable to form tetramers in MEKO cells, although alternate assemblies (e.g., hexamers) with channel activity could possibly form (Figure 4D). MEKO cells were stably transfected with each concatemer together with MICU1-FLAG to ensure sufficient MICU1. Three clones were identified for each condition, and whole-cell lysates were analyzed for MCU and MICU1/2-hetero-dimer expression by western blot (Figures S4B–S4D). Surprisingly, the MMMME construct failed to express (Figure S4E). Thus, to create channels with a single EMRE subunit/MCU tetramer, the MMME concatemer and MICU1-FLAG were expressed in EMRE KO (HEK293T) cells (Figure 4E) and three stable clones were isolated as described. The presence of endogenous MCU in these cells should allow a single MCU monomer to associate with the MMME concatemer to form tetrameric channel complexes containing only one EMRE subunit. Indeed, the MMME concatemer only very weakly expressed in MEKO cells, whereas it expressed well in EMRE KO cells (Figures 4F and 4G), suggesting that endogenous MCU interacted with and stabilized MMME expression. To probe the integrity of each concatemer, mitochondria were isolated from selected clones and analyzed by western blot. The ME[P76I], MME, and MMME (in EMRE KO cells) concatemers were all predominantly expressed as full-length proteins (ME~40 kDa; MME~80 kDa, and MMME~110 kDa, respectively, Figures 4F and 4G). Localization of each concatemer and MICU1-FLAG to mitochondria was confirmed by confocal immunofluorescence microscopy (Figure 4H). It was possible to compare MCU expression in ME[P76I] clones with that in WT cells as this concatemer exhibited a single band in western blots and contained a single MCU epitope. ME[P76I] was ~2-fold overexpressed in one clone (#3), modestly (<2-fold) overexpressed in a second (#1), and slightly lower (~2-fold) than WT cells in a third (#2) (Figure S4C). The presence of high-molecular-weight bands in cells expressing MME and MMME made it difficult to assess the relative MCU levels. This was further confounded by possible differences in MCU-antibody binding to fusion proteins containing multiple MCU subunits. We therefore employed V5-epitope ELISA assays on each clonal cell line. Based on the relationship in ME[P76I] clone #2 between western blot expression and the relative number of V5-binding sites per cell, the MCU expression level was estimated to vary by only 2-fold among the different concatemer clones (Figure S5A). MICU1/2 dimer expression in all clones was at least as high as in WT cells (Figure S4D).

We assessed mitochondrial Ca^{2+} uptake in each cell line at both high (5–8 μM) and low (<600 nM) $[Ca^{2+}]_c$ to determine (1) whether each concatemer was sufficient to form functional channels in the absence of endogenous MCU or EMRE expression and (2) if the channels exhibited normal MICU1/2-mediated gatekeeping. Each concatemer reconstituted MCU activity, with some variability among clones in the Ca^{2+}-uptake rates (ranging from ~100 to 400 nM/s) in response to 5-μM Ca^{2+} boluses (Figure S5B). Six of twelve clones displayed intact gatekeeping at low (<600 nM) $[Ca^{2+}]_c$ (Figure S5C). We selected individual clones for each concatemeric construct that had mean Ca^{2+}-uptake rates at 5–8 μM $[Ca^{2+}]_c$ most similar to WT cells and intact gatekeeping in the low-$[Ca^{2+}]_c$ regime (Figures S5A–S5C, red arrows). For each, we measured Ca^{2+}-uptake rates in response to 0.1–10 μM $[Ca^{2+}]_c$ and the subsequent steady-state $[Ca^{2+}]_c$ at which gatekeeping was re-established (Figures 5A–5D). Plotting uptake rate as a function of the peak $[Ca^{2+}]_c$ immediately after Ca^{2+} addition and fitting the data to a Hill equation revealed similar profiles for the different concatemers, with the rate for cells expressing ME[P76I] notably right-shifted to higher $[Ca^{2+}]_c$ (Figure 5E).

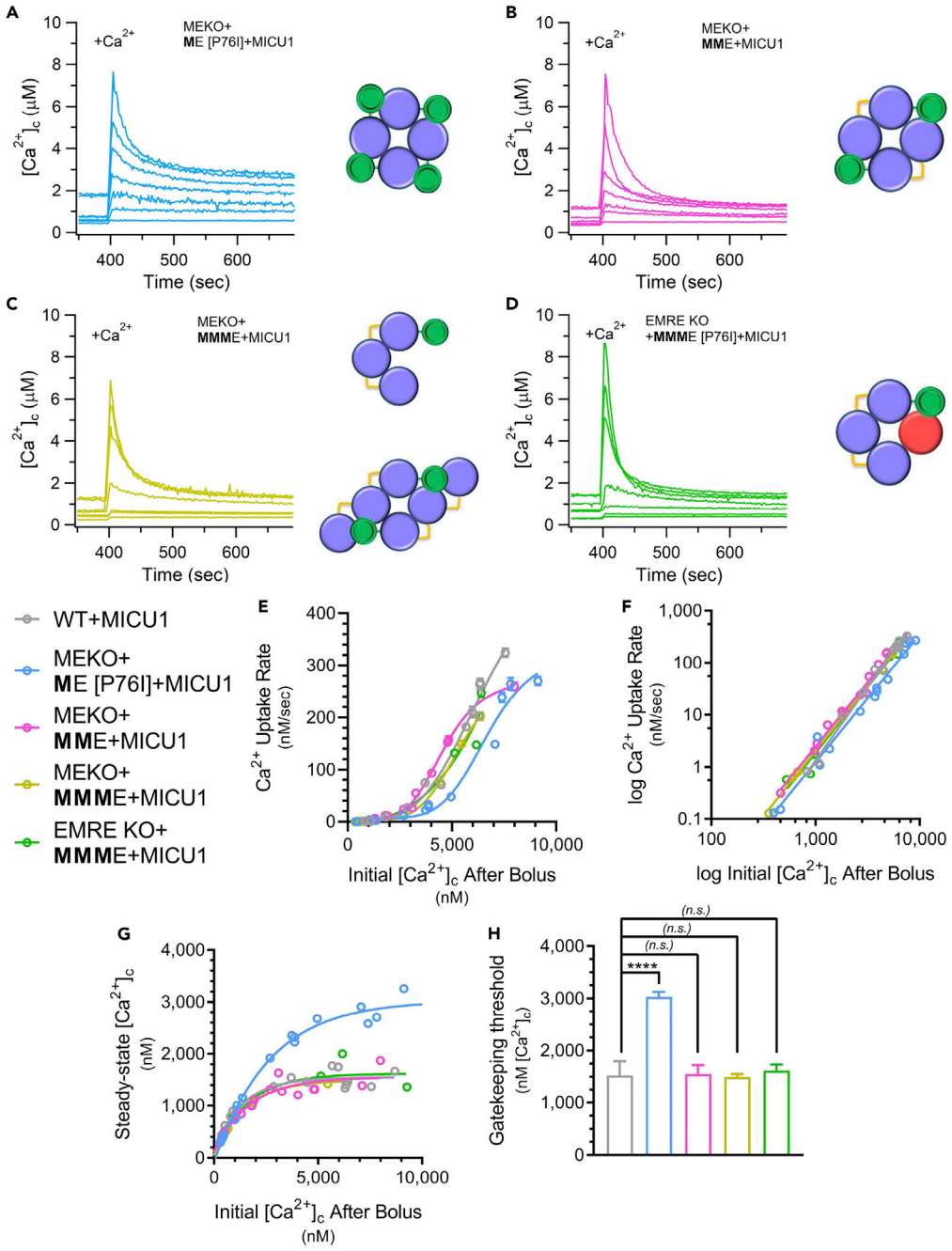

Figure 5. Function of MCU-EMRE Concatemers

(A–D) Mitochondrial Ca^{2+} uptake in MEKO + ME[P76I]+MICU1 (A), MEKO + MME + MICU1 (B), MEKO + MMME + MICU1 (C), and EMRE KO + MMME + MICU1 (D) cells in response to acute increases of $[Ca^{2+}]_c$ to between 0.1 and 10 μM. Individual traces from independent experiments with different bolus additions shown.

(E) Ca^{2+}-uptake rates for cell lines in (A)–(D) in response to challenge with $[Ca^{2+}]_c$ between 0.1 and 10 μM. Each point (hollow circle) represents independent experiment. Solid lines: Hill equation fits of Ca^{2+}-uptake rate versus initial $[Ca^{2+}]_c$ after bolus addition. ME[P76I]+MICU1 cells exhibited a right shift in the $[Ca^{2+}]_c$ dependence of MCU activation compared with all other cell lines.

(F) Ca^{2+}-uptake rates between 0.1 and 10 μM $[Ca^{2+}]_c$ measured in (E) plotted on $\log_{10}/\log_{10}$ scale. Each point (hollow circle) represents independent experiment. Solid lines: linear fits of ($\log_{10}$) Ca^{2+}-uptake rate versus ($\log_{10}$) $[Ca^{2+}]_c$. Slope of the best-fit line as a measure of cooperative MCU activation similar among all cell lines.

Figure 5. *Continued*

(G) Steady-state $[Ca^{2+}]_c$ for cells in (E) measured 300 s after bolus addition of 0.1–10 μM Ca^{2+} plotted as a function of initial peak $[Ca^{2+}]_c$. Each point (hollow circle) represents independent experiment ($n \geq 6$ for each condition). Solid lines: one-phase association fits of steady-state gatekeeping-threshold $[Ca^{2+}]_c$ versus initial $[Ca^{2+}]_c$ after addition.

(H) Comparison of gatekeeping-threshold $[Ca^{2+}]_c$ 300 s after bolus additions of Ca^{2+} from non-linear fits in (G). Bars: mean of plateau parameter for each fit ±SEM. p Values: pairwise comparisons with WT + MICU1 cells (****$p < 0.0001$; n.s., not different; Tukey's multiple comparisons test). Gatekeeping threshold was elevated in ME[P76I]+MICU1 cells compared with other cell lines.

See also Figure S5.

Linear fits on a log/log scale showed that cooperativity in the transition of MCU from the closed to the open state was the same for each concatemer (slope = 2.5), and similar to WT + MICU1 cells (Figure 5F), suggesting that MICU1/2 regulation was properly coupled to the channel in each concatemer complex. Importantly, however, the threshold at which gatekeeping was re-established (Figure 5G) was elevated uniquely in cells expressing ME[P76I] (Figure 5H). This result is consistent with the right-shifted Ca^{2+} dependence of MCU activation observed in these cells, and it suggests that gatekeeping is particularly potent in MCU complexes containing four EMRE/channel. In contrast, gatekeeping thresholds in cells expressing concatemers predicted to form channels with fewer than four EMRE subunits were not different from those of WT (+MICU1) cells (Figure 5H). These results strongly suggest that channels containing four EMRE subunits tether more MICU1/2 dimers to the channel complex than are normally present in WT cells, consistent with the analysis above that also suggested that EMRE:MCU stoichiometry, and by analogy the MICU1/2 dimer:MCU stoichiometry, may not be 4:4 or invariant in cells.

Biochemical Analyses of MCU-EMRE Complexes

To compare the relative sizes of MCU-EMRE concatemer and endogenous channel complexes, we performed BN-PAGE western blotting of MCU from isolated mitochondria. The MCU complex in WT cells ran as a single band at ~440 kDa (Figures 6A, 6C, 6D, and 6F: black), in line with previous reports (Sancak et al., 2013) (König et al., 2016). Overexpression of MICU1-FLAG in WT cells had no effect on the size of the complex (Figures 6A, 6C, 6D, and 6F: gray). In addition, MCU ran at approximately the same size in MICU1-KO mitochondria as in WT mitochondria (Figures 6A, 6C, 6D, and 6F: red), with a minor band of lower molecular weight similar in size to that observed in EMRE-KO mitochondria (~350 kDa) (Figures 6A, 6C, 6D, and 6F: orange). These results are consistent with a previous report that MICU1 may stabilize interactions between MCU and EMRE and that MCU-containing bands at ~440 kDa do not contain MICU proteins (König et al., 2016). Re-probing the blots with an α-FLAG antibody revealed that MICU1 assembled in complexes of ~250 and ~400 kDa in the absence of MCU and EMRE (Figure 6B), further indicating that complexes at ~440 kDa detected with the α-MCU antibody contained only MCU and EMRE subunits.

Importantly, complexes from mitochondria expressing ME[P76I] with an enforced 1:1 EMRE:MCU stoichiometry (Figures 6A, 6C, 6E, and 6F: blue) were significantly larger (~490 kDa) than those observed in WT or WT + MICU1 mitochondria. Accounting for the V5 tag, the size of the ME concatemer differs from that of one MCU and one fully processed EMRE subunit by ~1 kDa. This small difference cannot account for the observed difference of ~20 kDa between the WT or WT + MICU1 complexes compared with the ME[P76I] complex. This result suggests that endogenous MCU channels contain fewer than four EMRE subunits. A minor band at ~700 kDa was observed in ME[P76I] mitochondria, possibly corresponding to a dimer of MCU tetramers. Bands at ~440 and ~700 kDa were also seen in mitochondria from cells expressing MME and MMME, although higher-molecular-weight oligomers were evident (Figures 6A and 6C: pink, gold, and green). This could indicate a tendency for the concatemers to form complexes containing more than one MCU channel. Bands for MMME were much stronger when the construct was expressed in EMRE KO cells than in MEKO cells, likely due to enhanced stability of MMME in the presence of MCU expression due to their biochemical interaction. The molecular weights of MME and MMME complexes were not different from that of the MCU complex in WT cells (Figures 6E and 6F: pink and gold). Importantly, MCU complexes in EMRE-KO cells expressing MMME, which are predicted to contain a single EMRE subunit, were significantly smaller than those in WT cells (Figures 6A, 6C, 6E, and 6F: green), suggesting that endogenous MCU channels associate with more than one EMRE.

DISCUSSION

The first important conclusion from this study is that human MCU complexes with fewer than four EMRE subunits can assemble as fully functional channels. This is evidenced by the finding that mitochondria from cells that have

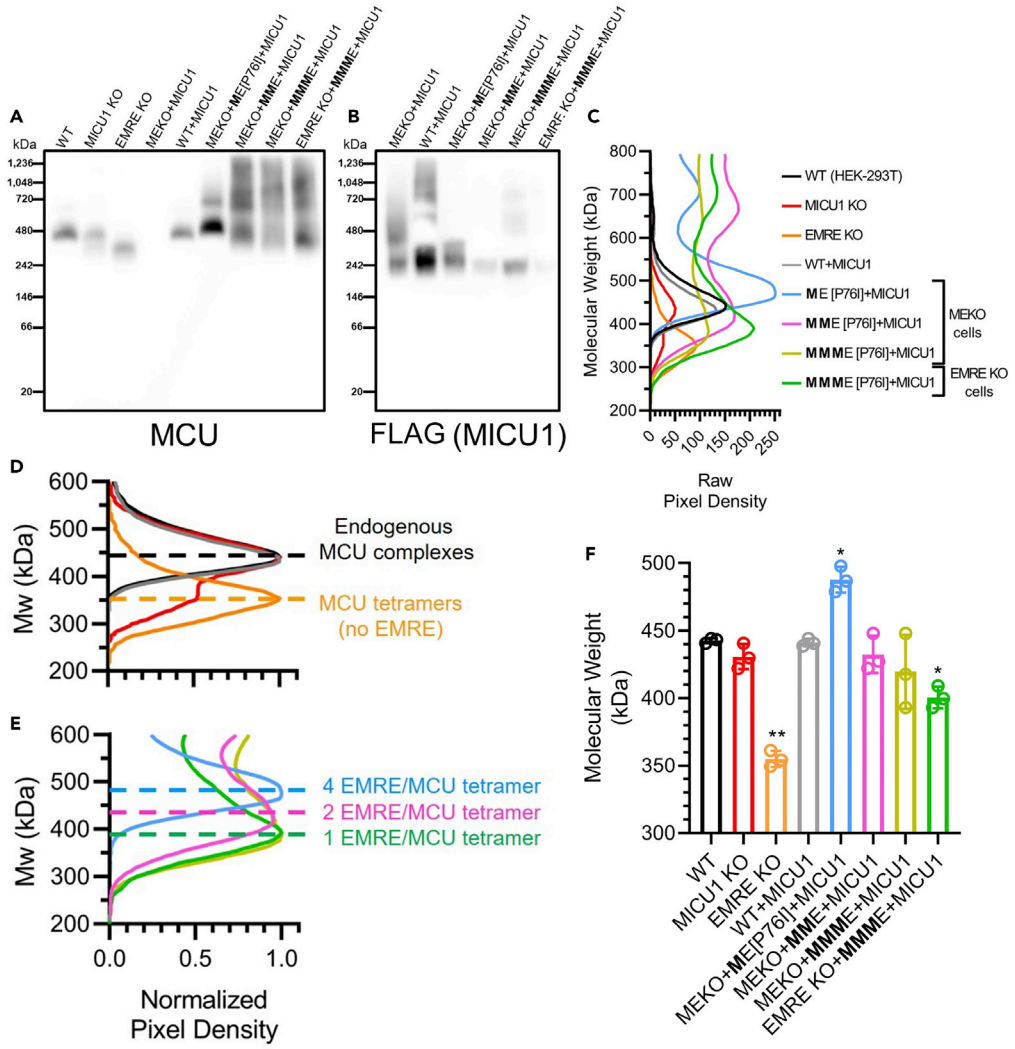

Figure 6. The Size of Concatemeric Channels Is Proportional to the Number of EMRE

(A) BN-PAGE MCU western blot of mitochondria isolated from WT, MICU1 KO, EMRE KO, MEKO + MICU1 cells and representative clones of WT + MICU1, MEKO + ME[P76I]+MICU1, MEKO + MME + MICU1, MEKO + MMME + MICU1, and EMRE-KO + MMME + MICU1 cells. Endogenous MCU complexes observed as single band at ~440 kDa.

(B) BN-PAGE western blot for FLAG (MICU1) in mitochondria isolated from representative clones as indicated. MICU1 in complexes at ~250 and ~400 kDa in cells lacking MCU and EMRE.

(C) Quantification of raw intensity and molecular weight from α-MCU BN-PAGE western blots in (A). Traces are mean of n = 3 replicate experiments. All MCU-EMRE concatemers showed bands between 300 and 600 kDa (similar to WT cells), as well as bands at >700 kDa that likely represent complexes containing >4 MCU subunits.

(D and E) Molecular weight profile of smallest band (200–600 kDa) from α-MCU BN-PAGE of cell lines in (C). Traces: mean of n = 3 replicate experiments; data normalized to band with maximal intensity for each condition. (D) MCU complexes in MICU1 KO cells (red) were similar to WT (+/− MICU1, black and gray), with a minor band similar in size to complexes formed in EMRE KO cells (orange). (E) MCU-EMRE concatemers exhibited molecular weights that varied in size proportionally to the predicted number of EMRE subunits per complex.

(F) Statistical analysis of molecular weight profiles in (D)–(E). Bars: mean calculated size of each complex derived from peak intensity of bands between 200 and 600 kDa ±SEM. Replicate measurements: hollow circles (n = 3). p Values: pairwise comparisons of each cell line with WT cells (*$p < 0.05$; **$p < 0.01$; Dunnett's multiple comparisons test). Complexes with four EMRE subunits per channel (ME[P76I], blue) were significantly larger than those in WT cells (black), whereas complexes containing only one EMRE subunit (EMRE KO + MMME, green) were smaller.

~10-fold higher expression of MCU relative to EMRE took up Ca^{2+} at rates similar to WT cells at $[Ca^{2+}]_c$ >5 μM (Figure 1) and further by the fact that MCU-EMRE concatemers that form channels with less than four EMRE subunits were functional (Figure 5). BN-PAGE revealed higher-order MCU oligomers in mitochondria expressing MME or MMME concatemers (Figure 6), but bands corresponding to MCU tetramers with one or two EMRE subunits (250–550 kDa) predominated. The BN-PAGE western blots revealed bands for MMME in EMRE KO cells corresponding to both an MCU tetramer (presumably containing endogenous MCU subunits) and a larger species, possibly corresponding to a hexamer (as depicted in Figure 3D). Expression of the MMME construct in the cells lacking MCU was very weak compared with expression in the EMRE KO cells that expressed MCU, suggesting that the endogenous MCU interacted with the MMME protein to stabilize its expression. This indicates that the dominant functional species in MME expressing cells was likely an MCU tetramer containing one EMRE. Thus, under circumstances where endogenous EMRE expression is insufficient to occupy all four binding sites in each channel, complexes with fewer than four EMREs retain full channel activity when the gatekeeping threshold is exceeded. Thus, we conclude that a 4 EMRE:1 channel stoichiometry is not necessarily *the* channel stoichiometry as suggested (Wang et al., 2019).

Second, the endogenous MCU channel in HEK293T cells likely contains two EMRE subunits. No differences in the $[Ca^{2+}]_c$ dependence of MCU activity or in the gatekeeping threshold were observed between channels with two EMRE subunits (MEKO + MME + MICU1) and WT cells (Figure 5), suggesting that these channels recapitulate the stoichiometry of endogenous channels. Of note, however, the functional profiles of cells expressing the MMME concatemer, which are predicted to form channels containing a single EMRE subunit, were functionally indistinguishable from those of MEKO + MME + MICU1 (or WT) cells. This could be due to formation of higher-order oligomers in the MMME-expressing cells (Figure 6) that created channels containing more than one EMRE, as depicted in Figure 4D. The $[Ca^{2+}]_c$ threshold for MCU activity in these cells likely arises from channels with one or two EMRE subunits. BN-PAGE analyses further suggested that endogenous MCU complexes run as a single species containing more than one and fewer than four EMRE per channel (Figure 6). The size of complexes between 250 and 550 kDa depended on the number of EMRE subunits per channel but not on incorporation of MICU proteins as they were not present in the complexes. Importantly, channels formed by expression of MME concatemers were not different in size from those in WT cells, whereas complexes containing a single EMRE were significantly smaller. Thus, the size of the native complex in WT cells is consistent with a channel complex containing two EMRE subunits bound to each MCU tetramer.

The third major conclusion is that gatekeeping is enhanced in MCU channels containing more EMRE subunits. Because the EMRE[P76I] mutation increased the steady-state expression of EMRE without affecting MCU expression (Figure 3), differences in channel function and regulation between MCU + EMRE + MICU1 and MCU + P76I-EMRE + MICU1 cells were due solely to the elevated EMRE:MCU ratio in the P76I-EMRE cells. Both cell lines showed similar uptake rates and cooperativity of channel activation, but the right shift in plots of initial uptake rate versus $[Ca^{2+}]_c$ and the elevated gatekeeping threshold in MCU + P76I-EMRE + MICU1 cells indicate that MICU1/2-mediated gatekeeping in channels with three or four EMRE is enhanced compared with those associated with only one or two. These findings are reinforced by the functional profile of the ME[P76I] concatemer, in which all channels are predicted to contain four EMRE (Figure 5). Like MCU + P76I-EMRE + MICU1 cells, ME[P76I]+MICU1 cells showed a right shift in the Ca^{2+}-uptake rate versus initial $[Ca^{2+}]_c$ relationship and an elevated gatekeeping threshold compared with WT + MICU1 cells, with no differences in uptake rate and cooperative activation.

These findings are relevant in light of the recent structure of human MCU that revealed four EMRE subunits bound to the MCU tetramer. We confirmed here that such a channel is functional with robust MICU1/2-mediated gatekeeping but that a 4:4 stoichiometry in not obligatory. Our results provide further evidence that EMRE performs two independent roles in MCU-channel regulation. First, it allows MCU to adopt an open channel conformation by binding only a single EMRE. In contrast, its role in tethering MICU1/2 to the complex to mediate channel gatekeeping is modulated by the number of EMRE subunits per channel. Such a phenomenon is reminiscent of the functional modulation of BK channels by auxiliary subunits γ1 and β (Gonzalez-Perez et al., 2018). Similar to the role of EMRE in MCU activation, γ1 has an "all-or-none" effect of the voltage dependence of BK-channel gating, in which a single subunit associating with the pore-forming subunits is sufficient to promote the full effect. On the other hand, each β-subunit that associates with the BK α-tetramer incrementally shifts the voltage-dependence of channel gating such that the full shift is observed only when four β-subunits are present in the channel complex.

Our studies suggest that the endogenous MCU-channel complex in HEK293T cells contains an MCU tetramer that, on average, associates with two or three EMRE subunits. We suggest that, under resting $[Ca^{2+}]_c$, two apo-MICU1/2 dimers associate with the complex through interactions with the C terminus of two EMRE subunits and residues in MCU subunits, mediating channel inhibition (i.e., gatekeeping). When the local $[Ca^{2+}]_c$ rises, Ca^{2+} binding to MICU1/2 promotes dissociation of MICU1 from the pore and relieves MCU inhibition. Under these conditions, a role of EMRE in tethering MICU1/2 dimers to the complex may be essential to ensure that gatekeeping is re-established quickly enough to ensure that channel activity ceases at the proper $[Ca^{2+}]_c$ threshold after uptake has occurred. Future work to address the structures of MCU channels with fewer than four EMRE subunits and the MCU-EMRE complex in the presence of MICU1/2 dimers is necessary to confirm these hypotheses.

Limitations of the Study

This study was performed using an immortalized line rather than primary cells from different tissues. Creating double (MCU, EMRE) knockout lines in primary cells is desirable to determine the relevance of the findings here in other cell types. However, such an undertaking is beyond the scope of this manuscript. The purpose of this study was not to characterize the assembly of MCU channel complexes in different tissues but rather to show in a single system which complexes are sufficient for channel activity and how the relative stoichiometry of MCU and EMRE affects channel function.

MCUb has been shown to form complexes with MCU (Raffaello et al., 2013), and some evidence suggests that MICU1/2 (and possibly EMRE) do not associate with MCUb (Lambert et al., 2019). Thus, it is possible that the preferred 2:4 EMRE:MCU channel stoichiometry we observe is due to formation of complexes with two MCU, two MCUb and two EMRE subunits that retain channel activity.

METHODS

All methods can be found in the accompanying Transparent Methods supplemental file.

SUPPLEMENTAL INFORMATION

Supplemental Information can be found online at https://doi.org/10.1016/j.isci.2020.101037.

ACKNOWLEDGMENTS

We thank Dr. Vamsi Mootha for providing the EMRE KO cell line. This work was supported by T32 HL 7954-16 (R.P.) and NIH R37 GM056238 (J.K.F.).

AUTHOR CONTRIBUTIONS

R.P. and J.K.F. conceived the project and wrote the manuscript. R.P. designed the experiments, performed the experiments, and analyzed the data. C.L. performed the experiments and analyzed the data.

DECLARATION OF INTERESTS

The authors declare that they have no conflicts of interest with the contents of this article.

Received: October 6, 2019
Revised: February 24, 2020
Accepted: April 1, 2020
Published: April 24, 2020

REFERENCES

Antony, A.N., Paillard, M., Moffat, C., Juskeviciute, E., Correnti, J., Bolon, B., Rubin, E., Csordás, G., Seifert, E.L., Hoek, J.B., et al. (2016). MICU1 regulation of mitochondrial Ca^{2+} uptake dictates survival and tissue regeneration. Nat. Commun. *7*, 10955.

Baradaran, R., Wang, C., Siliciano, A.F., and Long, S.B. (2018). Cryo-EM structures of fungal and metazoan mitochondrial calcium uniporters. Nature *559*, 580–584.

Baughman, J.M., Perocchi, F., Girgis, H.S., Plovanich, M., Belcher-Timme, C.A., Sancak, Y., Bao, X.R., Strittmatter, L., Goldberger, O., Bogorad, R.L., et al. (2011). Integrative genomics identifies MCU as an essential component of the mitochondrial calcium uniporter. Nature *476*, 341–345.

Fan, C., Fan, M., Orlando, B.J., Fastman, N.M., Zhang, J., Xu, Y., Chambers, M.G., Xu, X., Perry, K., Liao, M., et al. (2018). X-ray and cryo-EM structures of the mitochondrial calcium uniporter. Nature *559*, 575–579.

Gonzalez-Perez, V., Ben Johny, M., Xia, X.-M., and Lingle, C.J. (2018). Regulatory γ1 subunits defy symmetry in functional modulation of BK

channels. Proc. Natl. Acad. Sci. U S A *115*, 9923–9928.

Hoffman, N.E., Chandramoorthy, H.C., Shamugapriya, S., Zhang, X., Rajan, S., Mallilankaraman, K., Gandhirajan, R.K., Vagnozzi, R.J., Ferrer, L.M., Sreekrishnanilayam, K., et al. (2013). MICU1 motifs define mitochondrial calcium uniporter binding and activity. Cell Rep. *5*, 1576–1588.

Kamer, K.J., Grabarek, Z., and Mootha, V.K. (2017). High-affinity cooperative Ca^{2+} binding by MICU1-MICU2 serves as an on-off switch for the uniporter. EMBO Rep. *18*, 1397–1411.

Kamer, K.J., and Mootha, V.K. (2014). MICU1 and MICU2 play nonredundant roles in the regulation of the mitochondrial calcium uniporter. EMBO Rep. *15*, 299–307.

Kirichok, Y., Krapivinsky, G., and Clapham, D.E. (2004). The mitochondrial calcium uniporter is a highly selective ion channel. Nature *427*, 360–364.

König, T., Tröder, S.E., Bakka, K., Korwitz, A., Richter-Dennerlein, R., Lampe, P.A., Patron, M., Mühlmeister, M., Guerrero-Castillo, S., Brandt, U., et al. (2016). The m-AAA protease associated with neurodegeneration limits MCU activity in mitochondria. Mol. Cell *64*, 148–162.

Kovács-Bogdán, E., Sancak, Y., Kamer, K.J., Plovanich, M., Jambhekar, A., Huber, R.J., Myre, M.A., Blower, M.D., and Mootha, V.K. (2014). Reconstitution of the mitochondrial calcium uniporter in yeast. Proc. Natl. Acad. Sci. U S A *111*, 8985–8990.

Lambert, J.P., Luongo, T.S., Tomar, D., Jadiya, P., Gao, E., Zhang, X., Lucchese, A.M., Kolmetzky, D.W., Shah, N.S., and Elrod, J.W. (2019). MCUB regulates the molecular composition of the mitochondrial calcium uniporter channel to limit mitochondrial calcium overload during stress. Circulation *140*, 1720–1733.

Lee, S.K., Shanmughapriya, S., Mok, M.C.Y., Dong, Z., Tomar, D., Carvalho, E., Rajan, S., Junop, M.S., Madesh, M., and Stathopulos, P.B. (2016). Structural insights into mitochondrial calcium uniporter regulation by divalent cations. Cell Chem. Biol. *23*, 1157–1169.

Liu, J.C., Liu, J., Holmström, K.M., Menazza, S., Parks, R.J., Fergusson, M.M., Yu, Z.-X., Springer, D.A., Halsey, C., Liu, C., et al. (2016). MICU1 serves as a molecular gatekeeper to prevent in vivo mitochondrial calcium overload. Cell Rep. *16*, 1561–1573.

Mallilankaraman, K., Doonan, P., Cárdenas, C., Chandramoorthy, H.C., Müller, M., Miller, R., Hoffman, N.E., Gandhirajan, R.K., Molgó, J., Birnbaum, M.J., et al. (2012). MICU1 is an essential gatekeeper for MCU-mediated mitochondrial Ca^{2+} uptake that regulates cell survival. Cell *151*, 630–644.

Nguyen, N.X., Armache, J.-P., Lee, C., Yang, Y., Zeng, W., Mootha, V.K., Cheng, Y., Bai, X.-C., and Jiang, Y. (2018). Cryo-EM structure of a fungal mitochondrial calcium uniporter. Nature *559*, 570–574.

Oxenoid, K., Dong, Y., Cao, C., Cui, T., Sancak, Y., Markhard, A.L., Grabarek, Z., Kong, L., Liu, Z., Ouyang, B., et al. (2016). Architecture of the mitochondrial calcium uniporter. Nature *533*, 269–273.

Paillard, M., Csordás, G., Huang, K.-T., Várnai, P., Joseph, S.K., and Hajnóczky, G. (2018). MICU1 interacts with the D-Ring of the MCU pore to control its Ca^{2+} flux and sensitivity to Ru360. Mol. Cell *72*, 778–785.e3.

Patron, M., Checchetto, V., Raffaello, A., Teardo, E., Vecellio Reane, D., Mantoan, M., Granatiero, V., Szabò, I., De Stefani, D., and Rizzuto, R. (2014). MICU1 and MICU2 finely tune the mitochondrial Ca^{2+} uniporter by exerting opposite effects on MCU activity. Mol. Cell *53*, 726–737.

Patron, M., Granatiero, V., Espino, J., Rizzuto, R., and De Stefani, D. (2019). MICU3 is a tissue-specific enhancer of mitochondrial calcium uptake. Cell Death Differ. *26*, 179–195.

Payne, R., Hoff, H., Roskowski, A., and Foskett, J.K. (2017). MICU2 restricts spatial crosstalk between $InsP_3R$ and MCU Channels by regulating threshold and gain of MICU1-mediated inhibition and activation of MCU. Cell Rep. *21*, 3141–3154.

Perocchi, F., Gohil, V.M., Girgis, H.S., Bao, X.R., McCombs, J.E., Palmer, A.E., and Mootha, V.K. (2010). MICU1 encodes a mitochondrial EF hand protein required for Ca^{2+} uptake. Nature *467*, 291–296.

Petrungaro, C., Zimmermann, K.M., Küttner, V., Fischer, M., Dengjel, J., Bogeski, I., and Riemer, J. (2015). The Ca^{2+}-dependent release of the Mia40-induced MICU1-MICU2 dimer from MCU regulates mitochondrial Ca^{2+} uptake. Cell Metab. *22*, 721–733.

Phillips, C.B., Tsai, C.-W., and Tsai, M.-F. (2019). The conserved aspartate ring of MCU mediates MICU1 binding and regulation in the mitochondrial calcium uniporter complex. Elife *8*, e41112.

Plovanich, M., Bogorad, R.L., Sancak, Y., Kamer, K.J., Strittmatter, L., Li, A.A., Girgis, H.S., Kuchimanchi, S., De Groot, J., Speciner, L., et al. (2013). MICU2, a paralog of MICU1, resides within the mitochondrial uniporter complex to regulate calcium handling. PLoS One *8*, e55785.

Raffaello, A., De Stefani, D., Sabbadin, D., Teardo, E., Merli, G., Picard, A., Checchetto, V., Moro, S., Szabò, I., and Rizzuto, R. (2013). The mitochondrial calcium uniporter is a multimer that can include a dominant-negative pore-forming subunit. EMBO J. *32*, 2362–2376.

Sancak, Y., Markhard, A.L., Kitami, T., Kovács-Bogdán, E., Kamer, K.J., Udeshi, N.D., Carr, S.A., Chaudhuri, D., Clapham, D.E., Li, A.A., et al. (2013). EMRE is an essential component of the mitochondrial calcium uniporter complex. Science *342*, 1379–1382.

Csordás, G., Golenár, T., Seifert, E.L., Kamer, K.J., Sancak, Y., Perocchi, F., Moffat, C., Weaver, D., de la Fuente Perez, S., Bogorad, R., et al. (2013). MICU1 controls both the threshold and cooperative activation of the mitochondrial Ca^{2+} uniporter. Cell Metab. *17*, 976–987.

De Stefani, D., Raffaello, A., Teardo, E., Szabò, I., and Rizzuto, R. (2011). A forty-kilodalton protein of the inner membrane is the mitochondrial calcium uniporter. Nature *476*, 336–340.

Tsai, C.-W., Wu, Y., Pao, P.-C., Phillips, C.B., Williams, C., Miller, C., Ranaghan, M., and Tsai, M.-F. (2017). Proteolytic control of the mitochondrial calcium uniporter complex. Proc. Natl. Acad. Sci. U S A *114*, 4388–4393.

Tsai, M.-F., Phillips, C.B., Ranaghan, M., Tsai, C.-W., Wu, Y., Willliams, C., and Miller, C. (2016). Dual functions of a small regulatory subunit in the mitochondrial calcium uniporter complex. Elife *5*, 1–17.

Wang, L., Yang, X., Li, S., Wang, Z., Liu, Y., Feng, J., Zhu, Y., and Shen, Y. (2014). Structural and mechanistic insights into MICU1 regulation of mitochondrial calcium uptake. EMBO J. *33*, 594–604.

Vais, H., Mallilankaraman, K., Mak, D.-O.D., Hoff, H., Payne, R., Tanis, J.E., and Foskett, J.K. (2016). EMRE is a matrix Ca^{2+} sensor that governs gatekeeping of the mitochondrial Ca^{2+} uniporter. Cell Rep. *14*, 403–410.

Wang, Y., Nguyen, N.X., She, J., Zeng, W., Yang, Y., Bai, X., and Jiang, Y. (2019). Structural mechanism of EMRE-dependent gating of the human mitochondrial calcium uniporter. Cell *177*, 1252–1261.e13.

Xing, Y., Wang, M., Wang, J., Nie, Z., Wu, G., Yang, X., and Shen, Y. (2019). Dimerization of MICU proteins controls Ca^{2+} influx through the mitochondrial Ca^{2+} uniporter. Cell Rep. *26*, 1203–1212.e4.

Yamamoto, T., Yamagoshi, R., Harada, K., Kawano, M., Minami, N., Ido, Y., Kuwahara, K., Fujita, A., Ozono, M., Watanabe, A., et al. (2016). Analysis of the structure and function of EMRE in a yeast expression system. Biochim. Biophys. Acta *1857*, 831–839.

Yoo, J., Wu, M., Yin, Y., Herzik, M.A., Lander, G.C., and Lee, S.-Y. (2018). Cryo-EM structure of a mitochondrial calcium uniporter. Science *361*, 506–511.

iScience, Volume *23*

Supplemental Information

Variable Assembly of EMRE and MCU Creates Functional Channels with Distinct Gatekeeping Profiles

Riley Payne, Carmen Li, and J. Kevin Foskett

SUPPLEMENTAL INFORMATION

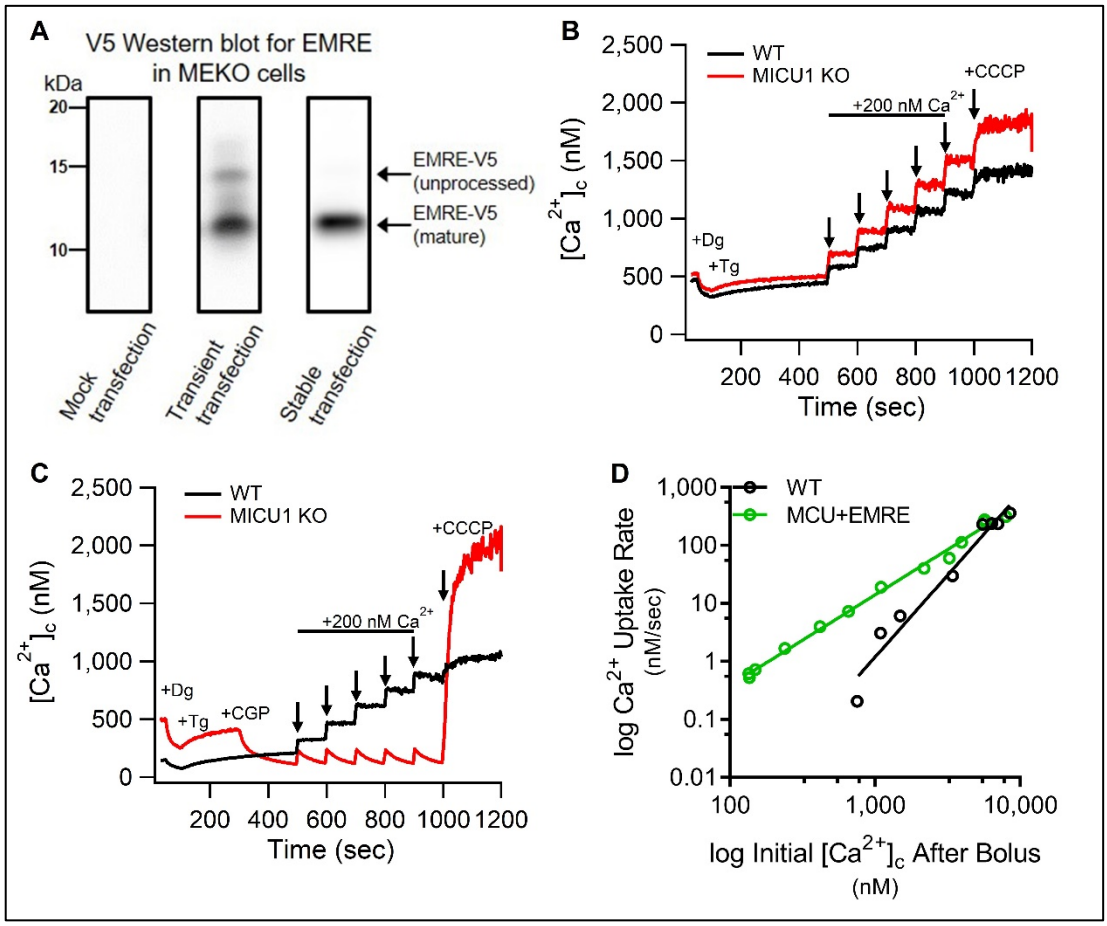

Figure S1. (Related to Figure 1)

(A) V5 western blots from whole-cell lysates of MEKO cells with no transfection, transient transfection, or stable transfection of EMRE-V5. Bands shown are from different blots; each result is representative of $n \geq 4$ biological replicates and $n \geq 3$ technical replicates for each condition. Transient expression of EMRE-V5 results in bands corresponding to both the unprocessed (~14 kDa) and mature (~11 kDa) forms of EMRE while cells with stable expression show only the mature form of EMRE. (B) Mitochondrial Ca^{2+} uptake in suspensions of permeabilized WT (HEK-293T) or MICU1 KO cells measured with the high-affinity indicator Fura-2 with no CGP37157 added to inhibit NCLX activity. A series of bolus addition of 200 nM free-Ca^{2+} are added beginning at t = 500 sec. 2 µM CCCP was added at t = 1000 sec to uncouple mitochondria and release matrix Ca^{2+}. Representative traces from $n \geq 3$ independent replicates for each cell line shown. No Ca^{2+} uptake observed in either cell line between 500 nM and 1.5 µM $[Ca^{2+}]_c$. (C) Mitochondrial Ca^{2+} uptake in suspensions of permeabilized cells performed as described in (B) with 20 µM CGP37157 added t = 300 sec. Representative traces from $n \geq 3$ independent replicates for each cell line shown. Inhibition of mitochondrial Ca^{2+} efflux through NCLX reveals constitutive MCU-mediated Ca^{2+} uptake at low $[Ca^{2+}]_c$ in MICU1 KO cells (red trace) whereas minimal uptake is observed in WT cells. (D) Ca^{2+}-uptake rates for WT and MCU+EMRE cells in response to acute challenge with $[Ca^{2+}]_c$ between 0.1 - 10 µM as a function of the $[Ca^{2+}]_c$ immediately after bolus addition plotted on a $\log_{10}/\log_{10}$ scale. Each point (hollow circle) represents an independent experiment. Solid lines: linear fits of Ca^{2+}-uptake rate vs. $[Ca^{2+}]_c$ to demonstrate cooperativity of MCU activation and highlight differences in Ca^{2+}-uptake rates at low (<1 µM) $[Ca^{2+}]_c$. Slope of the best-fit line is related to the cooperativity of the transition of MCU from the closed to the open state, which is reduced in MCU+EMRE cells (slope = 1.6) relative to WT cells (slope = 2.8).

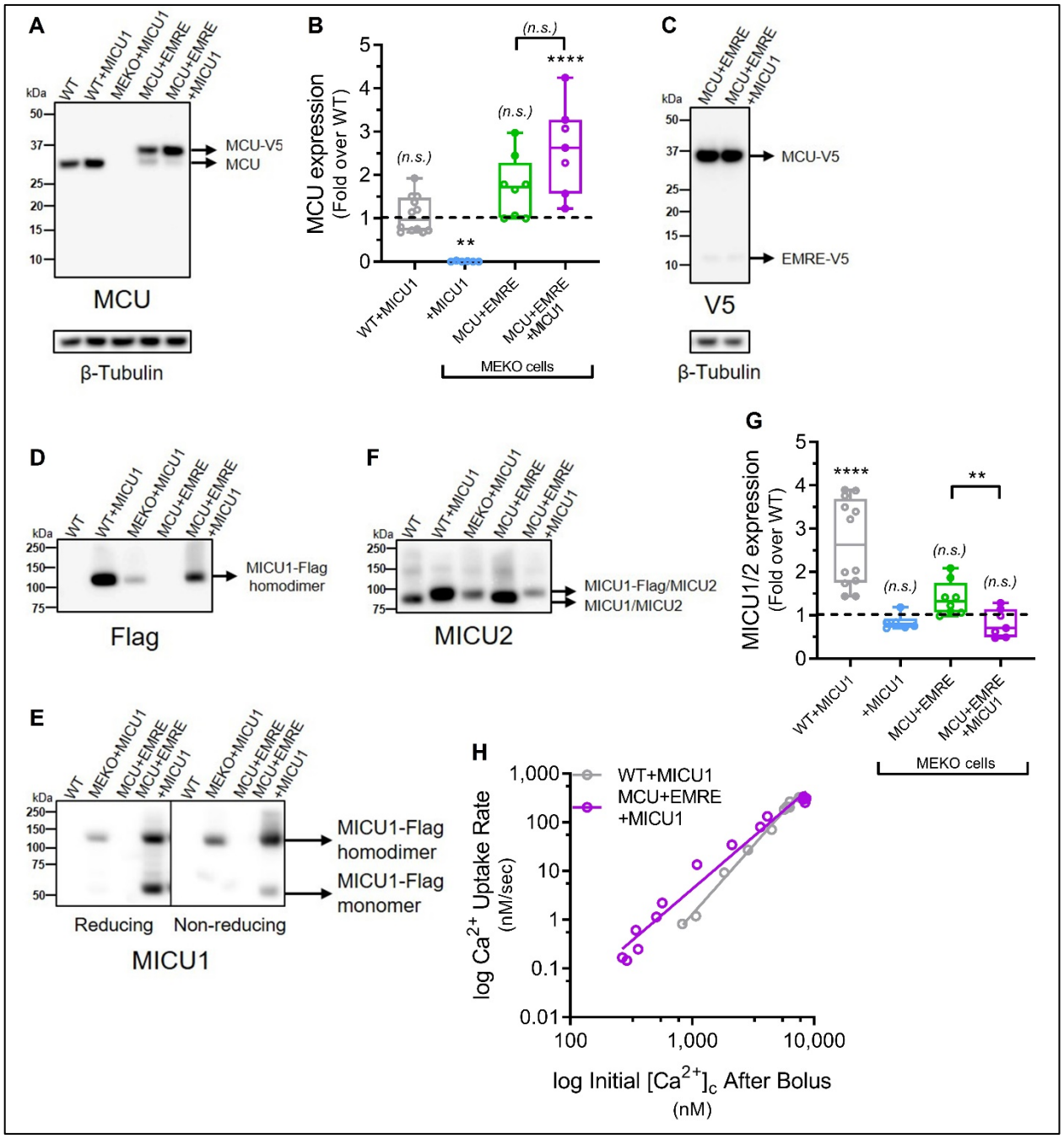

Figure S2. (Related to Figure 2)

(A) Western blot for MCU and β-tubulin from whole-cell lysates of WT, WT+MICU1, MEKO+MICU1, MCU+EMRE and MCU+EMRE+MICU1 cells under reducing conditions. (B) Quantification of MCU western blot band intensity for cell lines in (A) from n ≥ 6 independent experiments. Mean pixel density corrected for β-tubulin intensity and normalized to endogenous MCU band intensity in WT cells for each experiment. Replicate measurements shown as hollow circles, boxes: the 25th-75th percentile with line at median, error bars represent range of all measurements. P-values above each box: pairwise comparisons of each cell line with WT cells (*P < 0.05; **P < 0.01; ***P < 0.001; ****P < 0.0001; n.s., not different; Dunnett's multiple comparisons test) and p-value above line spanning green and purple bars: pairwise comparison of MCU+EMRE and MCU+EMRE+MICU1 cells (unpaired t test with Welch's correction). (C) Western blot for V5 and β-tubulin from whole-cell lysates of MCU+EMRE and MCU+EMRE+MICU1 cells under reducing conditions. EMRE-V5 evident as a dim band at ~11 kDa while dark bands at ~35 kDa represent MCU-V5. (D) Western blot for Flag (MICU1) for cell lines in (B) under non-reducing conditions to preserve MICU1 homodimers (~110 kDa). (E) Western blot for MICU1 in mitochondria isolated from WT, MEKO+MICU1, MCU+EMRE and MCU+EMRE+MICU1 cells under reducing (left) and non-reducing conditions to preserve MICU1 homodimers (~110 kDa) (right). Expression of MICU1-Flag exceeds that of endogenous MICU1. (F) Western blot for MICU2 for cell lines

in (A) under non-reducing conditions to preserve MICU1/2 heterodimers. Increase in molecular weight from 90 kDa to 100 kDa with MICU1-Flag expression is due to formation of MICU1-Flag/MICU2 heterodimers. (G) Quantification of MICU2 western blot band intensity for cell lines in (A) from $n \geq 6$ independent experiments as described in (B). Replicate measurements shown as hollow circles, boxes: the 25^{th}-75^{th} percentile with line at median, error bars: range of all measurements. P-values: pairwise comparisons of each cell line with WT cells (*P < 0.05; **P < 0.01; ***P < 0.001; ****P < 0.0001; n.s., not different; Dunnett's multiple comparisons test. P-value above line spanning green and purple bars: pairwise comparison of MCU+EMRE and MCU+EMRE+MICU1 cells (unpaired t test with Welch's correction). (H) Ca^{2+}-uptake rates for WT+MICU1 and MCU+EMRE+MICU1 cells in response to acute challenge with $[Ca^{2+}]_c$ between 0.1 - 10 μM as a function of the $[Ca^{2+}]_c$ immediately after bolus addition plotted on $\log_{10}/\log_{10}$ scale. Each point (hollow circle) represents an independent experiment. Solid lines: linear fits of Ca^{2+}-uptake rate vs. $[Ca^{2+}]_c$. Cooperativity of MCU activation is identical between WT and WT+MICU1 cells (slope = 2.8), while MCU+EMRE+MICU1 cells show increased cooperativity (slope = 2.1) relative to MCU+EMRE cells (slope = 1.6).

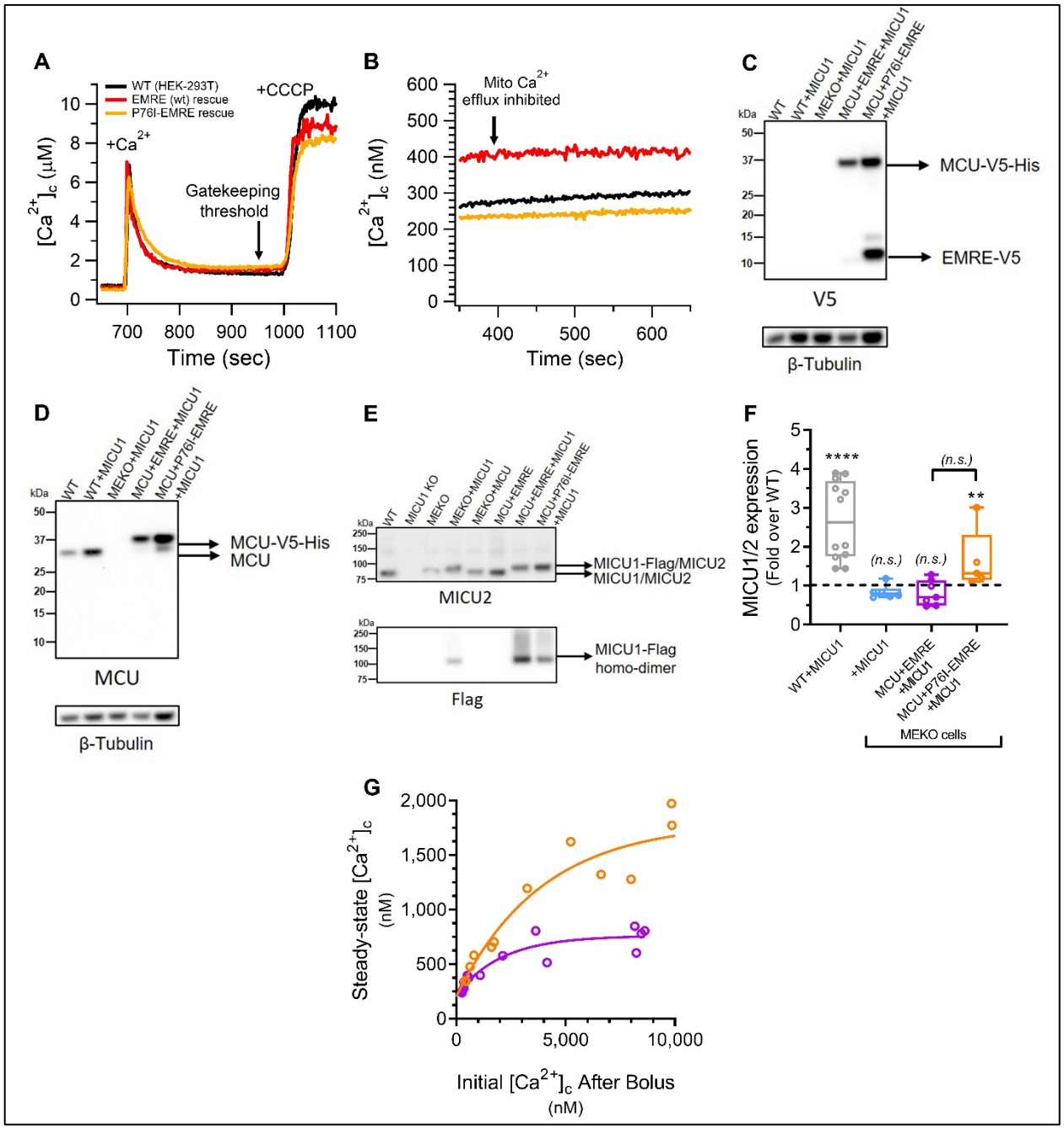

Figure S3. (Related to Figure 3)

(A) Mitochondrial Ca^{2+} uptake in suspensions of permeabilized WT (black trace) or EMRE KO cells stably expressing either EMRE-V5 (red trace) or P76I-EMRE-V5 (orange trace) in response to acute 5-μM increases of $[Ca^{2+}]_c$. Traces representative of $n \geq 3$ independent experiments. (B) $[Ca^{2+}]_c$ response to acute addition of CGP37157 to inhibit NCLX-mediated Ca^{2+} efflux for cell lines in (A) measured with the high-affinity indicator Fura-2. No uptake below 500 nM $[Ca^{2+}]_c$ observed in any of the cell lines tested. (C) Western blot for V5 and β-tubulin from whole-cell lysates of WT, WT+MICU1, MEKO+MICU1, MCU+EMRE+MICU1 MCU+P76I-EMRE+MICU1cells under reducing conditions. (D) Western blot for MCU and β-tubulin from whole-cell lysates of cell lines in (C) under reducing conditions. (E) Western blot for MICU2 (top) and Flag (MICU1 - bottom) from whole-cell lysates of WT, MICU1 KO, MEKO, MEKO+MICU1, MEKO+MCU, MCU+EMRE, MCU+EMRE+MICU1 and MCU+P76I-EMRE+MICU1 cells under non-reducing conditions. (F) Quantification of MICU2 western blot band intensity for WT+MICU1, MEKO+MICU1, MCU+EMRE+MICU1 and MCU+P76I-EMRE+MICU1 cells from $n \geq 5$ independent experiments. Mean pixel density corrected for β-tubulin intensity and normalized to endogenous MICU2 band intensity in WT cells for each experiment. Replicate measurements shown as hollow circles, boxes: the 25th-75th percentile with line at median, error bars: range of all measurements. P-values above each box: pairwise comparisons of each cell line with WT cells (*$P < 0.05$; **$P < 0.01$; ***$P < 0.001$; ****$P < 0.0001$; n.s.,

not different; Dunnett's multiple comparisons test). P-value above line spanning green and purple bars: pairwise comparison of MCU+EMRE+MICU1 and MCU+P76I-EMRE+MICU1 cells (unpaired t test with Welch's correction). (G) Steady-state $[Ca^{2+}]_c$ for MCU+EMRE+MICU1 and MCU+P76I-EMRE+MICU1 cells measured 300 sec after bolus addition of 0.1 - 10 μM Ca^{2+} plotted as function of the initial peak $[Ca^{2+}]_c$ achieved immediately after addition. Each point (hollow circle) represents an independent experiment ($n \geq 12$ for each condition). Solid lines: one-phase association fits of steady-state $[Ca^{2+}]_c$ vs. the initial $[Ca^{2+}]_c$ after addition.

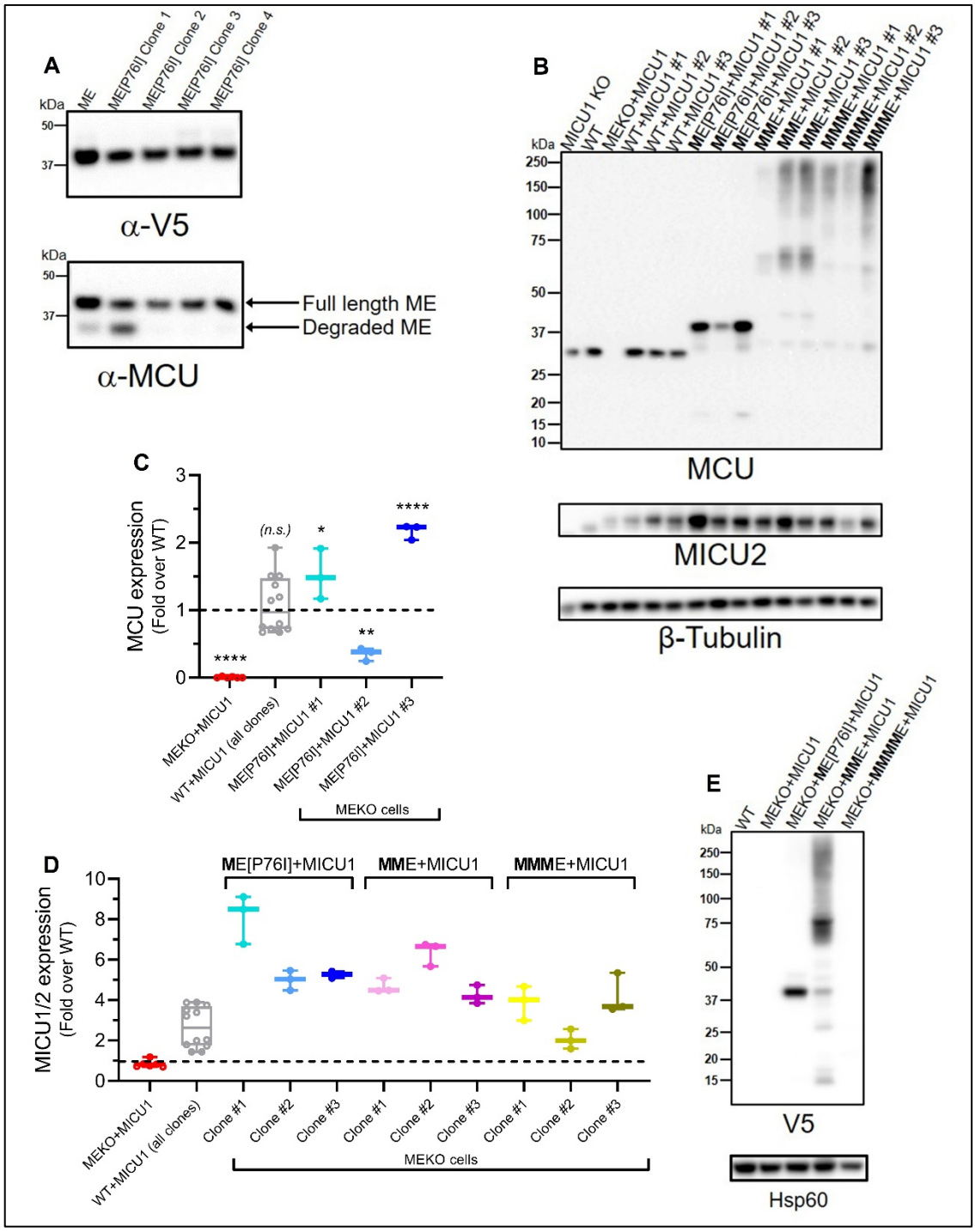

Figure S4. (Related to Figure 4)

(A) Western blot for V5 (top) and MCU (bottom) for whole-cell lysates of clonal MEKO cells stably-expressing ME (wt) (lane 1) or ME[P76I] (lanes 2-5). The EMRE [P76I] mutation prevents degradation of the ME concatemer in three of four clones. (B) Western blot for MCU, MICU2 (under non-reducing conditions) and β-tubulin from whole-cell lysates of WT, MEKO+MICU1, three clones of WT+MICU1, and three clones each of MEKO cells expressing ME[P76I]+MICU1, MME+MICU1, or MMME+MICU1. MICU1-Flag overexpression in each clone is evident from increased molecular weight of MICU1/2 dimers under non-reducing conditions. (C) Quantification of MCU western blot band intensity from whole-cell lysates of WT, MEKO+MICU1, WT+MICU1 and three clones of MEKO+ME[P76I]+MICU1 cells from $n \geq 3$ independent experiments. Mean pixel density corrected for β-tubulin intensity and normalized to endogenous MCU band intensity in WT+MICU1 cells for each experiment. Replicate measurements shown as hollow circles, boxes: the 25th-75th percentile with line at median, error bars: range of all measurements. P-values: pairwise comparisons of each cell line with WT cells (*P < 0.05; **P < 0.01; ***P < 0.001; ****P < 0.0001; n.s., not different; Dunnett's multiple comparisons test).

(D) Quantification of MICU2 western blot band intensity for cells in (B) from $n \geq 3$ independent experiments quantified as described in (C). Total MICU1/2 dimer expression is higher than WT in all cell lines expressing MICU1-Flag. (E) Western blot for V5 and Hsp60 of isolated mitochondria from representative clones of WT+MICU1, MEKO+MICU1, MEKO+ME[P76I]+MICU1, MEKO+MME+MICU1 and MEKO+MMMME+MICU1 cells under reducing conditions. No detectable MMMME expression observed.

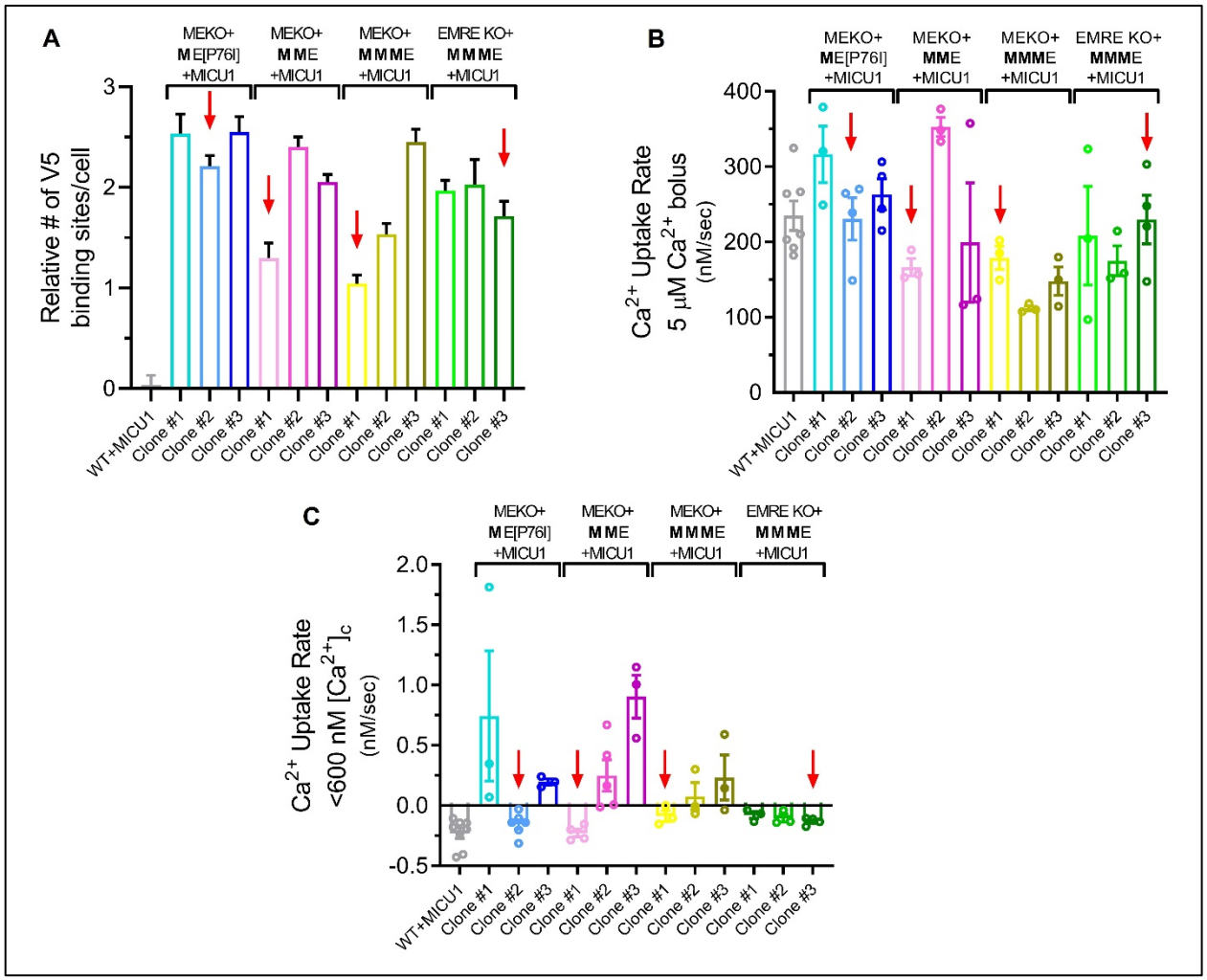

Figure S5. (Related to Figure 5)

(A) Quantification of V5 expression by ELISA for three clones each of WT+MICU1 (pooled), MEKO+ME[P76I]+MICU1, MEKO+MME+MICU1, MEKO+MMME+MICU1 and EMRE KO+MMME+MICU1. Bars: mean of B_{max} parameter for each fit +/- SEM (n = 3). Red arrows: lowest expressing clone for each condition. (B) Quantification of mitochondrial Ca^{2+}-uptake rates in response to bolus additions to raise $[Ca^{2+}]_c$ by 5 µM for cell lines in (A). Each point represents initial Ca^{2+}-uptake rate from an independent experiment ($n \geq 3$ for each condition) determined by single-exponential fit to reduction of $[Ca^{2+}]_c$. Replicate measurements shown as hollow circles, bars: mean +/- SEM. Clones with mean uptake rates most closely approximating WT for each condition shown by red arrows. (C) Quantification of mitochondrial Ca^{2+}-uptake rate below 600 nM $[Ca^{2+}]_c$ in response to inhibition of NCLX-mediated Ca^{2+} efflux for cell lines in (A). Each point represents initial Ca^{2+}-uptake rate from an independent experiment ($n \geq 3$ for each condition) determined by single-exponential fit to reduction of $[Ca^{2+}]_c$. Replicate measurements shown as hollow circles, bars: mean +/- SEM. Clones with uptake rates < 0 nM/sec (denoted by red arrows) exhibit intact gatekeeping at low $[Ca^{2+}]_c$.

TRANSPARENT METHODS

CONTACT FOR REAGENT AND RESOURCE SHARING

Further information and requests for resources and reagents should be directed to and will be fulfilled by the lead contact, J. Kevin Foskett (foskett@pennmedicine.upenn.edu).

EXPERIMENTAL MODEL AND SUBJECT DETAILS

Generation and maintenance of cell lines used

HEK293T cells from ATCC (ATTC Cat# CRL-3216, RRID: CVCL_0063) grown in DMEM containing 5-10% fetal bovine serum (Corning Cat# MT35-010-CV) and 1x antibiotic/antimycotic (Invitrogen Cat# 15240062) (complete medium) at 37˚C and 5% CO_2. EMRE KO (HEK293T) cells were a generous gift from Dr. Vamsi Mootha. All genomic copies of *MCU* were inactivated in EMRE KO cells using CRISPR/Cas9-mediated gene editing. sgRNAs targeting the 5' end of the *MCU* coding sequence were chosen using MIT CRISPR guide design tool (Zhang Lab, http://crispr.mit.edu). Two *guides* were chosen to target Exon 1 (guides 1 and 2) and two for Exon 2 (guides 3 and 4).

Guide 1 (5'-3'):

(Forward) CAGGAGCGATCTACCTGCGG; (Reverse) CCGCAGGTAGATCGCTCCTG

Guide 2 (5'-3'):

(Forward) CAGCAGGAGCGATCTACCTG; (Reverse) CAGGTAGATCGCTCCTGCTG

Guide 3 (5'-3'):

(Forward) TGACAGCGTTCACGCCGGGA; (Reverse) TCCCGGCGTGAACGCTGTCA

Guide 4 (5'-3'):

(Forward) TGAACTGACAGCGTTCACGC; (Reverse) GCGTGAACGCTGTCAGTTCA

Oligonucleotides were annealed, treated with T4 polynucleotide kinase (NEB Cat# M0201S) at 37ºC for 30 min, 95ºC for 5 min, and ramped from 95-25ºC (5ºC/min), and ligated into the pSpCas9(BB)-2A-GFP (PX458) vector (RRID: Addgene_48138) that had been digested with BbsI (NEB Cat# #R3539) and treated with calf intestinal alkaline phosphatase (NEB Cat# M0290). Ligation reactions were performed using T4 DNA ligase (NEB Cat# M0202S) and used to transform Turbo competent *E. coli* (NEB Cat# C2984H). Individual clones were isolated and the presence of each sgRNA was verified by sequencing. Maxi prep DNA for each sgRNA pair was used to transfect EMRE KO (HEK293T) using TransIT®-LT1 transfection reagent (Mirus Cat# 2300) as per the manufacturer's protocol. One week after transfection individual GFP-positive cells isolated at the Wistar Institute flow cytometry facility and select clones were grown to confluence in 10 cm dishes. Loss of MCU expression in each clone was verified by western blot and genomic sequencing. cDNAs of full-length V5-tagged EMRE and Flag-tagged MICU1 were obtained from Origene in both the pCMV6-A-BSD (Origene Cat# PS100022) and pCMV6-A-Puro (Origene Cat# PS100025) vectors. pDEST40-MCU-V5-HIS was purchased from Addgene (RRID: Addgene_31731) and subcloned into pCMV6-A-BSD and pCMV6-A-Puro using NotI (NEB Cat# R0189S) and PmeI (NEB Cat# R0560S) restriction enzymes and standard molecular biology techniques described above. P76I-EMRE-V5 cDNA in pCMV6-A-BSD and pCMV6-A-Puro were generated using the QuickChange II XL site-directed mutagenesis kit (Stratagene Cat# 200521) and XL10-Gold® ultracompetent *E. Coli* (Stratagene Cat#200314). The MCU-EMRE concatemer described by Tsai et al. (2016) with and without the EMRE[P76I] mutation in pCMV6-A-BSD and pCMV6-A-Puro were created using a PCR-based cloning strategy. Fusion proteins with additional MCU subunits fused to EMRE were synthesized and sequence-verified by Bio Basic Inc. and subcloned into pCMV6-A-Puro. Each additional MCU subunit added to the MCU-EMRE concatemer was encoded by a unique cDNA sequence to ensure stability of the construct and facilitate full-length sequencing (see Supplemental Information for sequences). Unique nucleotide sequences were generated using an algorithm (see Supplemental Information for code syntax) in the software R (R Core Team, 2018) using the Biostrings package (Pagès et al., 2017). Stable cell lines were created by transfection as previously described and maintained in complete medium with 5 µg/mL blasticidin (Invitrogen Cat# R21001) and/or 2 µg/mL puromycin (Thermo Fisher Scientific Cat# 540222) until stable expression of each plasmid was achieved. Clones were isolated by limiting dilution for each condition and maintained in complete medium with antibiotics. Importantly, we screened numerous clones for each line created to select the ones for experimentation that had expression levels of expressed proteins most similar to the endogenous ones.

Amino acid sequences encoded by cDNAs used in this study

Human EMRE (C-terminal V5 tag):

MASGAARWLVLAPVRSGALRSGPSLRKDGDVSAAWSGSGRSLVPSRSVIVTRSGAILPKPVKMSFGLLRVFSIVIPFLYVGTL
ISKNFAALLEEHDIFVPEDDDDDDGKPIPNPLLGLDST

Human P76I-EMRE (C-terminal V5 tag):

MASGAARWLVLAPVRSGALRSGPSLRKDGDVSAAWSGSGRSLVPSRSVIVTRSGAILPKPVKMSFGLLRVFSIVIIFLYVGTLI
SKNFAALLEEHDIFVPEDDDDDDGKPIPNPLLGLDST

Human MCU (C-terminal V5-(6x)His tag):

MAAAAGRSLLLLLSSRGGGGGGAGGCGALTAGCFPGLGVSRHRQQQHHRTVHQRIASWQNLGAVYCSTVVPSDDVTVVY
QNGLPVISVRLPSRRERCQFTLKPISDSVGVFLRQLQEEDRGIDRVAIYSPDGVRVAASTGIDLLLLDDFKLVINDLTYHVRPP
KRDLLSHENAATLNDVKTLVQQLYTTLCIEQHQLNKERELIERLEDLKEQLAPLEKVRIEISRKAEKRTTLVLWGGLAYMAT
QFGILARLTWWEYSWDIMEPVTYFITYGSAMAMYAAYFVMTRQEYVYPEARDRQYLLFFHKGAKKSRFDLEKYNQLKDAIA
QAEMDLKRLRDPLQVHLPLRQIGEKDCPTFLYKVVDLEGPRFEGKPIPNPLLGLDSTRTGHHHHHH

Human MICU1 (C-terminal Myc-Flag tag):

MFRLNSLSALAELAVGSRWYHGGSQPIQIRRRLMMVAFLGASAVTASTGLLWKRAHAESPPCVDNLKSDIGDKGKNKDEG
DVCNHEKKTADLAPHPEEKKKKRSGFRDRKVMEYENRIRAYSTPDKIFRYFATLKVISEPGEAEVFMTPEDFVRSITPNEKQP
EHLGLDQYIIKRFDGKKISQEREKFADEGSIFYTLGECGLISFSDYIFLTTVLSTPQRNFEIAFKMFDLNGDGEVDMEEFEQVQS
IIRSQTSMGMRHRDRPTTGNTLKSGLCSALTTYFFGADLKGKLTIKNFLEFQRKLQHDVLKLEFERHDPVDGRITERQFGGML
LAYSGVQSKKLTAMQRQLKKHFKEGKGLTFQEVENFFTFLKNINDVDTALSFYHMAGASLDKVTMQQVARTVAKVELSDH
VCDVVFALFDCDGNGELSNKEFVSIMKQRLMRGLEKPKDMGFTRLMQAMWKCAQETAWDFALPKQTRTRPLEQKLISEED
LAANDILDYKDDDDK

MCU-EMRE concatemer (C-terminal V5 tag):

MAAAAGRSLLLLLSSRGGGGGGAGGCGALTAGCFPGLGVSRHRQQQHHRTVHQRIASWQNLGAVYCSTVVPSDDVTVVY
QNGLPVISVRLPSRRERCQFTLKPISDSVGVFLRQLQEEDRGIDRVAIYSPDGVRVAASTGIDLLLLDDFKLVINDLTYHVRPP
KRDLLSHENAATLNDVKTLVQQLYTTLCIEQHQLNKERELIERLEDLKEQLAPLEKVRIEISRKAEKRTTLVLWGGLAYMAT
QFGILARLTWWEYSWDIMEPVTYFITYGSAMAMYAAYFVMTRQEYVYPEARDRQYLLFFHKGAKKSRFDLEKYNQLKDAIA
QAEMDLKRLRDPLQVHLPLRQIGEKDVSAAWSGSGRSLVPSRSVIVTRSGAILPKPVKMSFGLLRVFSIVIPFLYVGTLISKNF
AALLEEHDIFVPEDDDDDDGKPIPNPLLGLDST

MCU-EMRE[P76I] concatemer (C-terminal V5 tag):

MAAAAGRSLLLLLSSRGGGGGGAGGCGALTAGCFPGLGVSRHRQQQHHRTVHQRIASWQNLGAVYCSTVVPSDDVTVVY
QNGLPVISVRLPSRRERCQFTLKPISDSVGVFLRQLQEEDRGIDRVAIYSPDGVRVAASTGIDLLLLDDFKLVINDLTYHVRPP
KRDLLSHENAATLNDVKTLVQQLYTTLCIEQHQLNKERELIERLEDLKEQLAPLEKVRIEISRKAEKRTTLVLWGGLAYMAT
QFGILARLTWWEYSWDIMEPVTYFITYGSAMAMYAAYFVMTRQEYVYPEARDRQYLLFFHKGAKKSRFDLEKYNQLKDAIA
QAEMDLKRLRDPLQVHLPLRQIGEKDVSAAWSGSGRSLVPSRSVIVTRSGAILPKPVKMSFGLLRVFSIVIIFLYVGTLISKNF
AALLEEHDIFVPEDDDDDDGKPIPNPLLGLDST

MCU-MCU-EMRE concatemer (C-terminal V5-tag):

MAAAAGRSLLLLLSSRGGGGGGAGGCGALTAGCFPGLGVSRHRQQQHHRTVHQRIASWQNLGAVYCSTVVPSDDVTVVY
QNGLPVISVRLPSRRERCQFTLKPISDSVGVFLRQLQEEDRGIDRVAIYSPDGVRVAASTGIDLLLLDDFKLVINDLTYHVRPP
KRDLLSHENAATLNDVKTLVQQLYTTLCIEQHQLNKERELIERLEDLKEQLAPLEKVRIEISRKAEKRTTLVLWGGLAYMAT
QFGILARLTWWEYSWDIMEPVTYFITYGSAMAMYAAYFVMTRQEYVYPEARDRQYLLFFHKGAKKSRFDLEKYNQLKDAIA
QAEMDLKRLRDPLQVHLPLRQIGEKDASGGSGGGSGGGSGVHQRIASWQNLGAVYCSTVVPSDDVTVVYQNGLPVISVRLP
SRRERCQFTLKPISDSVGVFLRQLQEEDRGIDRVAIYSPDGVRVAASTGIDLLLLDDFKLVINDLTYHVRPPKRDLLSHENAAT
LNDVKTLVQQLYTTLCIEQHQLNKERELIERLEDLKEQLAPLEKVRIEISRKAEKRTTLVLWGGLAYMATQFGILARLTWWE
YSWDIMEPVTYFITYGSAMAMYAAYFVMTRQEYVYPEARDRQYLLFFHKGAKKSRFDLEKYNQLKDAIAQAEMDLKRLRDP
LQVHLPLRQIGEKDVSAAWSGSGRSLVPSRSVIVTRSGAILPKPVKMSFGLLRVFSIVIIFLYVGTLISKNFAALLEEHDIFVPED
DDDDDGKPIPNPLLGLDST

MCU-MCU-MCU-EMRE concatemer (C-terminal V5-tag):

MAAAAGRSLLLLLSSRGGGGGGAGGCGALTAGCFPGLGVSRHRQQQHHRTVHQRIASWQNLGAVYCSTVVPSDDVTVVY
QNGLPVISVRLPSRRERCQFTLKPISDSVGVFLRQLQEEDRGIDRVAIYSPDGVRVAASTGIDLLLLDDFKLVINDLTYHVRPP
KRDLLSHENAATLNDVKTLVQQLYTTLCIEQHQLNKERELIERLEDLKEQLAPLEKVRIEISRKAEKRTTLVLWGGLAYMAT
QFGILARLTWWEYSWDIMEPVTYFITYGSAMAMYAAYFVMTRQEYVYPEARDRQYLLFFHKGAKKSRFDLEKYNQLKDAIA
QAEMDLKRLRDPLQVHLPLRQIGEKDASGGSGGGSGGGSGVHQRIASWQNLGAVYCSTVVPSDDVTVVYQNGLPVISVRLPSR
RERCQFTLKPISDSVGVFLRQLQEEDRGIDRVAIYSPDGVRVAASTGIDLLLLDDFKLVINDLTYHVRPPKRDLLSHENAATL
NDVKTLVQQLYTTLCIEQHQLNKERELIERLEDLKEQLAPLEKVRIEISRKAEKRTTLVLWGGLAYMATQFGILARLTWWEY
SWDIMEPVTYFITYGSAMAMYAAYFVMTRQEYVYPEARDRQYLLFFHKGAKKSRFDLEKYNQLKDAIAQAEMDLKRLRDPL
QVHLPLRQIGEKDASGGSGGGSGGGSGVHQRIASWQNLGAVYCSTVVPSDDVTVVYQNGLPVISVRLPSRRERCQFTLKPIS
DSVGVFLRQLQEEDRGIDRVAIYSPDGVRVAASTGIDLLLLDDFKLVINDLTYHVRPPKRDLLSHENAATLNDVKTLVQQLY

TTLCIEQHQLNKERELIERLEDLKEQLAPLEKVRIEISRKAEKRTTLVLWGGLAYMATQFGILARLTWWEYSWDIMEPVTYFI
TYGSAMAMYAYFVMTRQEYVYPEARDRQYLLFFHKGAKKSRFDLEKYNQLKDAIAQAEMDLKRLRDPLQVHLPLRQIGE
KDVSAAWSGSGRSLVPSRSVIVTRSGAILPKPVKMSFGLLRVFSIVIIFLYVGTLISKNFAALLEEHDIFVPEDDDDDDGKPIPN
PLLGLDST

MCU-MCU-MCU-MCU-EMRE concatemer (C-terminal V5-tag):

MAAAAGRSLLLLLSSRGGGGGGAGGCGALTAGCFPGLGVSRHRQQQHHRTVHQRIASWQNLGAVYCSTVVPSDDVTVVY
QNGLPVISVRLPSRRERCQFTLKPISDSVGVFLRQLQEEDRGIDRVAIYSPDGVRVAASTGIDLLLLDDFKLVINDLTYHVRPP
KRDLLSHENAATLNDVKTLVQQLYTTLCIEQHQLNKERELIERLEDLKEQLAPLEKVRIEISRKAEKRTTLVLWGGLAYMAT
QFGILARLTWWEYSWDIMEPVTYFITYGSAMAMYAYFVMTRQEYVYPEARDRQYLLFFHKGAKKSRFDLEKYNQLKDAIA
QAEMDLKRLRDPLQVHLPLRQIGEKDASGGSGGGSGGGVHQRIASWQNLGAVYCSTVVPSDDVTVVYQNGLPVISVRLPSR
RERCQFTLKPISDSVGVFLRQLQEEDRGIDRVAIYSPDGVRVAASTGIDLLLLDDFKLVINDLTYHVRPPKRDLLSHENAATL
NDVKTLVQQLYTTLCIEQHQLNKERELIERLEDLKEQLAPLEKVRIEISRKAEKRTTLVLWGGLAYMATQFGILARLTWWEY
SWDIMEPVTYFITYGSAMAMYAYFVMTRQEYVYPEARDRQYLLFFHKGAKKSRFDLEKYNQLKDAIAQAEMDLKRLRDPL
QVHLPLRQIGEKDASGGSGGGSGGGVHQRIASWQNLGAVYCSTVVPSDDVTVVYQNGLPVISVRLPSRRERCQFTLKPISDS
VGVFLRQLQEEDRGIDRVAIYSPDGVRVAASTGIDLLLLDDFKLVINDLTYHVRPPKRDLLSHENAATLNDVKTLVQQLYTT
LCIEQHQLNKERELIERLEDLKEQLAPLEKVRIEISRKAEKRTTLVLWGGLAYMATQFGILARLTWWEYSWDIMEPVTYFITY
GSAMAMYAYFVMTRQEYVYPEARDRQYLLFFHKGAKKSRFDLEKYNQLKDAIAQAEMDLKRLRDPLQVHLPLRQIGEKD
ASGGSGGGSGGGSGVHQRIASWQNLGAVYCSTVVPSDDVTVVYQNGLPVISVRLPSRRERCQFTLKPISDSVGVFLRQLQEE
DRGIDRVAIYSPDGVRVAASTGIDLLLLDDFKLVINDLTYHVRPPKRDLLSHENAATLNDVKTLVQQLYTTLCIEQHQLNKER
ELIERLEDLKEQLAPLEKVRIEISRKAEKRTTLVLWGGLAYMATQFGILARLTWWEYSWDIMEPVTYFITYGSAMAMYAYF
VMTRQEYVYPEARDRQYLLFFHKGAKKSRFDLEKYNQLKDAIAQAEMDLKRLRDPLQVHLPLRQIGEKDVSAAWSGSGRS
LVPSRSVIVTRSGAILPKPVKMSFGLLRVFSIVIIFLYVGTLISKNFAALLEEHDIFVPEDDDDDDGKPIPNPLLGLDST

METHOD DETAILS

Simultaneous Determination of Ca^{2+} Uptake and $\Delta\Psi m$

Concurrent measurement of mitochondrial Ca^{2+} uptake and IMM potential ($\Delta\Psi_m$) in permeabilized HEK-293T cells was performed as described (Payne et al., 2017). Cells were grown in 10-cm tissue-culture coated dishes for 48 hr prior to each experiment. 6-8×10^6 cells were trypsinized, counted, and washed in a Ca^{2+}-free extracellular-like medium, centrifuged, suspended in 1.5 mL of intracellular-like medium (ICM - in mM: 120 KCl (Millipore-Sigma, Cat# P9333), 10 NaCl, 1 KH_2PO_4 (Millipore-Sigma Cat# P5655), 20 HEPES (Millipore-Sigma Cat# H3375), and 5 succinate (Millipore-Sigma Cat# S3674) [pH 7.2]) that had been treated with BT Chelex® 100 resin (Bio-Rad Cat# 143-2832) prior to use to attain an initial free [Ca^{2+}] of ~20 nM, and transferred to a cuvette. The cuvette was placed in a temperature-controlled (37°C) experimental compartment of a multi-wavelength-excitation dual wavelength-emission high-speed spectrofluorometer (Delta RAM, Photon Technology International). Membrane-impermeable Fura2 K^+ salt (Invitrogen Cat# F1200 - K_D = 140 nM) or FuraFF K^+ salt (AAT Bioquest Cat# 21028 - K_D = 5.5 µM) (final concentration 1 µM) and TMRE (Invitrogen Cat# T669) (final concentration 1 µM) were added at 25 sec to measure bath [Ca^{2+}]$_c$ and $\Delta\Psi_m$ concurrently. Fluorescence at 549-nm excitation/595-nm emission for TMRE, along with 340-nm and 380-nm excitation/535-nm emission for Fura2/FuraFF, was measured at 5 Hz. 40 µg/mL digitonin was added at 50 sec to permeabilize cells and allow the cytoplasm to equilibrate with the bath solution such that the degree of quenching of TMRE fluorescence reports the relative $\Delta\Psi_m$. Fura2/FuraFF fluorescence under these conditions is related to the cytoplasmic [Ca^{2+}] ([Ca^{2+}]$_c$) per the equation below, where (**R**) is the measured fluorescence ratio (340/380 nm), (**R_{min}**) is the fluorescence ratio under 0-[Ca^{2+}], (**R_{max}**) is the fluorescence ratio under saturating [Ca^{2+}], (**Sf_2**) and (**Sb_2**) are the absolute 380 nm excitation/535 nm emission fluorescence under 0-[Ca^{2+}] and saturating [Ca^{2+}], respectively, and (**K_D**) is the dissociation constant of the dye for Ca^{2+}.

$$[Ca^{2+}] = \left(\frac{R - R_{min}}{R_{max} - R}\right)\left(\frac{Sf_2}{Sb_2}\right) * K_D$$

Thapsigargin (Millipore-Sigma Cat# T9033) (2 µM) was added at 100 sec to inhibit Ca^{2+} uptake into the endoplasmic reticulum (ER) and CGP37157 (Tocris Cat# 1114) (20 µM; determined empirically in the assay to ensure complete inhibition of NCLX) was added either concurrently with thapsigargin or at 400 sec to inhibit NCLX-mediated mitochondrial Ca^{2+} extrusion. After [Ca^{2+}]$_c$ reached a steady state at 300 sec after CGP37157 addition, MCU-mediated Ca^{2+} uptake was initiated by adding boluses of 1-8 µL of either 0.5 or 5 mM $CaCl_2$ to the cuvette to achieve increases in [Ca^{2+}]$_c$ between ~100 nM and 10 µM. Differences in the initial [Ca^{2+}]$_c$ between 200-800 nM prior to bolus addition were due to unavoidable variability between replicates, but did not affect the Ca^{2+} uptake rate after bolus addition. Initial [Ca^{2+}]$_c$ greater than 10 µM after bolus addition was not performed because uptake rates were too fast for accurate measurement of the initial [Ca^{2+}]$_c$. Thus, the apparent plateau in the initial (peak) [Ca^{2+}]$_c$ achieved after addition is at least partially due to these limitations, as well as possible effects on $\Delta\Psi_m$ resulting from Ca^{2+} influx. The volume of $CaCl_2$ required to achieve the desired increase in [Ca^{2+}]$_c$ for each addition was calculated based on the activity coefficient for Ca^{2+} in ICM. Differences between the target [Ca^{2+}]$_c$ and the observed value recorded immediately after addition were due to unavoidable sources of experimental variability, including K_D limitations of Fura2 and pipetting errors. After [Ca^{2+}]$_c$ was monitored for 300 sec following

addition of each Ca^{2+} bolus, 2 µM CCCP (Millipore-Sigma Cat# C2759) was added to uncouple $\Delta\Psi_m$ and allow unimpeded Ca^{2+} efflux from mitochondria as a measure of the total extent of uptake. Under our conditions, Ca^{2+} boluses of >1 µM cause a transient depolarization as measured with TMRE that recovered after ~50-60 sec. Initial Ca^{2+} uptake rates in permeabilized cells were determined for each experiment using single-exponential fits from the time of CGP37157 or Ca^{2+} addition (t = 0 sec) to achievement of a new steady state (t = 300 sec) to obtain parameters **A** (extent of uptake) and **τ** (time constant) (IGOR Pro; RRID:SCR_000325). The instantaneous rate of uptake (**R**) at t = 0 is equal to the first derivative of the fit, and standard deviations (**SD**) of rates were calculated from standard deviations of **A** ($\mathbf{SD_A}$) and **τ** ($\mathbf{SD_\tau}$) as follows:

$$R = A/\tau \qquad R+SD = (A+SD_A)/(\tau-SD_\tau) \quad \text{and} \quad R-SD = (A-SD_A)/(\tau+SD_\tau)$$

For determination of the steady-state $[Ca^{2+}]_c$ after completion of uptake, the calculated $[Ca^{2+}]_c$ 300 sec after challenge with 0.1 - 10 µM Ca^{2+} (**Y**) was plotted as a function of the (peak) initial $[Ca^{2+}]_c$ achieved after bolus Ca^{2+} addition (**X**). Data were fitted using a one-phase association model where ($\mathbf{Y_0}$) is the Y value when X is zero, (**P**) is the plateau, or Y value at infinite X, and (**K**) is the rate constant, expressed in reciprocal of the X axis.

$$Y = Y_0 + (P - Y_0)(1 - e^{(-KX)})$$

The value of (**P**) represents to the steady-state $[Ca^{2+}]_c$ at which gatekeeping is re-established +/- the standard error of (**P**) determined from the fit.

SDS-PAGE western blotting

For western blotting of whole-cell lysates, cells grown in complete medium at 37°C and 5% CO_2 were washed with DPBS (Mediatech Cat# MT21-031-CM), detached with Versene solution (Thermo Fisher Scientific Cat# 15040066) and lysed with buffer containing (in mM): 50 Tris-HCl (pH 7.5 - Thermo Fisher Scientific SKU# 15567-027), 150 NaCl (Millipore-Sigma Cat# S9888), 0.05 EGTA (Sigma-Aldrich Cat# 03780), and 0.3 $CaCl_2$ (Ricca Cat# R1780000) with 0.2% (w/v) n-Dodecyl β-D-maltoside (Millipore-Sigma Cat# D4641). Immediately prior to use, lysis buffer was supplemented with 1 mM PMSF (Millipore-Sigma Cat# 10837091001) and cOmplete protease inhibitor cocktail (Roche Cat# 11697498001). For western blots of mitochondrial proteins, mitochondria were isolated as described (Sancak et al., 2013). Total protein concentrations were calculated using BCA Protein Assay kit (Thermo Fisher Scientific Cat# 23225), and samples for PAGE were prepared in 2x Laemmli sample buffer (Bio-Rad Cat# 1610737) +/- 2-Mercaptoethanol (βME) (Bio-Rad Cat# 1610710). NuPAGE© gels (4-12% - Thermo Fisher Scientific Cat# NP0321) were transferred to Immobilon© P PVDF membranes (Millipore-Sigma Cat# IPVH00010) and probed with various antibodies. Antibodies used: anti-MCU (Cell Signaling Technology Cat# 14997S), anti-V5 tag (Cell Signaling Technology Cat# 13202S), anti-MICU2 (Abcam Cat# ab101465), anti-DYKDDDDK (Flag tag) (Cell Signaling Technology Cat# 14793S), anti-MICU1 (Cell Signaling Technology Cat# 12524S) anti-β-Tubulin (Invitrogen Cat# 32-2600), and anti-Hsp60 (Abcam Cat# ab46798). Membranes were blocked in 5% fat-free milk for 1 hr at RT, incubated overnight at 4°C with primary antibody, and then for 1 hr at RT with anti-rabbit IgG-HRP (Cell Signaling Technology Cat# 7074S) or anti-mouse IgG-HRP (Cell Signaling Technology Cat# 7076S) secondary antibodies conjugated to horseradish peroxidase (HRP). Chemiluminescence detection was carried out using SuperSignal West Chemiluminescent Substrate (Thermo Fisher Scientific Cat# 34580). The mean pixel density of bands was quantified using the Fiji software package in ImageJ (ImageJ, RRID: SCR_003070), corrected for the intensity of the loading-control band (β-tubulin for whole-cell lysates or Hsp60 for isolated mitochondria), and normalized to the response in WT cells. For EMRE:MCU ratio calculations, the mean pixel density of the EMRE-V5 band was divided by the mean pixel density of the MCU-V5 band for each independent experiment. Predicted stoichiometry histograms were derived from the binomial probability equation where (**n**) is the number of possible combinations of EMRE and MCU that can assemble, (**r**) is the EMRE:MCU expression ratio determined from V5 western blot band intensities, and (**x**) is the number of EMRE subunits per channel.

$$P(x) = \frac{(n!)(r^x)((1-r)^{(n-x)})}{(x!)((n-x)!)}$$

P(x) is the probability of obtaining each channel stoichiometry based on the EMRE:MCU expression ratio given random association of the two proteins. A simple binary distribution was applied based on the assumption that binding of individual EMRE subunits to MCU tetramers is non-cooperative. Given cooperative assembly of EMRE and MCU, there would be a strong bias for a 1:1 EMRE:MCU stoichiometry among all functional channel complexes. If this were the case, a large deficit in total EMRE expression relative to MCU would lead to a reduction in the total number of functional channels and thus a slower rate of Ca^{2+} uptake, which was not observed (e.g. MCU+EMRE cells in which the EMRE:MCU expression ratio is ~1:10).

BN-PAGE western blotting

Total protein concentrations of isolated mitochondrial preparations were determined using BCA Protein Assay kit. 5 µg total protein of each sample for PAGE were prepared in 4x NativePAGE© sample buffer (Invitrogen Cat# BN2003) supplemented with 5% digitonin (Invitrogen Cat# BN2006). NativePAGE© gels (4-12% - Invitrogen Cat# BN1002) were either stained with Brilliant blue (R) protein stain (Millipore-Sigma Cat# B7920) (as a loading control and to detect NativeMark™ unstained protein standard

(Invitrogen Cat# LC0725)) or transferred to Immobilon© P PVDF membranes, fixed in 8% acetic acid, and probed with anti-MCU or anti-DYKDDDDK (Flag tag) antibodies. Membranes were blocked in 5% fat-free milk for 1 hr at RT, incubated overnight at 4°C with primary antibody, and then for 1 hr at RT with anti-rabbit IgG-HRP secondary antibody conjugated to HRP. Chemiluminescence detection was carried out as described above.

Determination of molecular weights for MCU-EMRE concatemers and native channels

Calibration of molecular weight was performed by plotting the peak intensity of each band of known molecular weight (**X**) from the marker as a function of the relative vertical position (**Y**) of each band on gels stained with Coomassie blue, and data were fitted using an exponential growth equation where ($\mathbf{Y_0}$) is the Y value when X is zero and (**K**) is the rate constant, expressed in reciprocal of the X axis:

$$Y = Y_0 \times e^{kX}$$

Pixel intensity for each lane in the MCU western blots sample was determined as previously described using Fiji, and molecular weights from n = 3 independent experiments were interpolated from the fit above.

Immunofluorescence microscopy of mitochondrial proteins

Clear 12-well tissue-culture treated plates (CytoOne Cat# CC7682-7524) were seeded with 2×10^5 cells/well on 12 mm glass coverslips in 500 µL/well of complete medium. Cells were grown for 24 hr prior to fixation in 1 mL of 4% (v/v) paraformaldehyde (Electron Microscopy Sciences Cat# 15713-S) in complete medium. Cells were fixed for 15 min at 37°C, washed with DPBS, and permeabilized in 1 mL/well of 0.1% (v/v) Triton X-100 detergent (Millipore-Sigma Cat# T8787) for 30 min at RT. Permeabilization solution was decanted and 2 mL of (2x) casein blocking buffer (Millipore-Sigma Cat# B6429) was added to each well and incubated for 30 min at RT. Blocking solution was removed and replaced with 1 mL/well of rabbit anti-V5 antibody and mouse anti-Flag M2 (Millipore-Sigma Cat# F3165) primary antibodies each diluted 1:2,000 in (1x) blocking buffer and incubated overnight at 4°C with gentle agitation. The following day plates were removed from 4°C, washed with 0.05% (v/v) Tween-20 (Bio-Rad Cat# 1706531) in DPBS, and 1 mL/well of anti-rabbit IgG Alexa Fluor 568-conjugated (Invitrogen Cat# A-11011) and anti-mouse IgG Alexa Fluor 488-conjugated (Invitrogen Cat# A-11001) secondary antibodies each diluted 1:2,000 in (1x) blocking buffer was added to each well and incubated in the dark for 1 hr at RT. Coverslips from each well were mounted on standard glass slides using VECTASHIELD® antifade mounting medium with DAPI (Vector Laboratories Cat# H-1200) and images were collected on a Leica TCS SP8 X system using a 100x/1.4 NA PL APO CS2 objective. Labeled V5-tagged proteins (MCU-EMRE concatemers) were excited using a continuously tunable white-light laser set to 568 nm to detect fluorescence emission between 600-700 nm. Labeled Flag-tagged proteins (MICU1-Flag) were excited at 488 nm to detect fluorescence emission between 510-550 nm. DAPI was excited at 408 nm to detect fluorescence emission between 430-470 nm.

In-cell ELISA to quantify V5 expression

Clear 96-well tissue-culture treated plates (Corning Cat# 3603) were seeded with 2.5×10^4 cells/well in 100 µL of complete medium. Each cell line was seeded in eight replicate wells across three replicate plates. Cells were grown for 24 hr then fixed, permeabilized and blocked as described above (200 µL/well). Blocking solution was removed and replaced with 100 µL/well of mouse anti-V5 antibody (Invitrogen Cat# R960-25) diluted in (1x) blocking buffer and incubated overnight at 4°C with gentle agitation. The following primary antibody dilutions were tested in triplicate wells: 1:1,000; 1:5,000, 1:25,000; 1:125,000; 1:250,000. One well for each cell line was reserved for the no-primary antibody control. The following day plates were removed from 4°C, washed as described above, and 100 µL/well of anti-mouse IgG HRP-linked secondary antibody diluted 1:2,000 in (1x) blocking buffer was added to each well and incubated for 1 hr at RT with gentle agitation. Secondary antibody was decanted, plates were washed as previously described, and 100 µL/well of 1-Step™ Ultra TMB - ELISA Substrate solution (Thermo Fisher Scientific Cat# 34028B) was added to each well and incubated for 10 min at RT. Absorbance at 650 nm of each well was measured in a Cytation 5 plate reader; three sequential measurements of each plate were made to ensure that the HRP reaction has reached completion. After reading, the substrate was removed and 50 µL of 0.3% (w/v) Janus Green B (Millipore-Sigma Cat# 201677) dye solution was added to each well as a control for cell density and plates were incubated for 5 min at RT. The dye was decanted, plates were washed with diH_2O to remove excess solution and 200 µL of 0.5 N HCl solution was added to each well. Absorbance at 595 nm was measured in the Cytation 5 plate reader as previously described. The ELISA signal (Abs @ 650 nm) for each well was normalized for cell density (Abs @ 595 nm) the mean normalized response for cell line was plotted as a function of the primary antibody dilution. Data were fitted in GraphPad Prism using a one site-total binding model where (**Y**) is the mean normalized ELISA response, ($\mathbf{B_{max}}$) is the relative total number of V5-binding sites, (**X**) is the primary antibody dilution factor, ($\mathbf{K_D}$) is the dissociation constant, (**NS**) represents the contribution of non-specific binding of the secondary antibody, and ($\mathbf{Y_0}$) is the background signal of the detector.

$$Y = \left[\frac{(B_{max})(X)}{K_D + X}\right] + (NS)(X) + Y_0$$

QUANTIFICATION AND STATISTICAL ANALYSIS

Independent, normally-distributed rate measurements and steady states after uptake were analyzed using ordinary one-way ANOVA and Tukey's multiple comparisons t-test to identify significant differences between all each cell line and all others. Normalized western blot band intensities were analyzed using ordinary one-way ANOVA and Dunnett's multiple comparisons t-test to identify differences in expression relative to WT cells, or Welch's unpaired t-test for pairwise comparisons between cell types other than WT. Molecular weight measurements from BN-PAGE western blots were analyzed using repeated measures one-way ANOVA and Dunnett's multiple comparisons t-test to identify differences relative to WT channel complexes. All statistical tests were performed using Prism v7.0 (GraphPad Prism, RRID:SCR_002798). P-values < 0.05(*); < 0.01(**); < 0.001(***); and < 0.0001(****) were considered statistically significant.

DATA AND CODE AVAILABILITY

R-code for unique nucleotide sequences from a given protein sequence

(Pages, H., Aboyoun, P., Gentleman, R., DebRoy, S., 2017. Biostrings: Efficient Manipulation of Biological Strings)

```
library(Biostrings)
cds<- DNAString("<ENTER FASTA AMINO ACID SEQUENCE HERE>")
cds
c<-codons(cds)

#Shuffle 1
#Valine
c1a<-gsub("GTA", "GTG", c, perl=TRUE)
c2a<-gsub("GTC", "GTA", c1a, perl=TRUE)
c3a<-gsub("GTT", "GTC", c2a, perl=TRUE)
        #Histidine
c4a<-gsub("CAC", "CAT", c3a, perl=TRUE)
        #Glutamine
c5a<-gsub("CAG", "CAA", c4a, perl=TRUE)
        #Arginine
c6a<-gsub("AGA", "CGG", c5a, perl=TRUE)
c7a<-gsub("AGG", "AGA", c6a, perl=TRUE)
c8a<-gsub("CGT", "AGG", c7a, perl=TRUE)
c9a<-gsub("CGC", "CGT", c8a, perl=TRUE)
c10a<-gsub("CGA", "CGC", c9a, perl=TRUE)
        #Isoleucine
c11a<-gsub("ATC", "ATA", c10a, perl=TRUE)
c12a<-gsub("ATT", "ATC", c11a, perl=TRUE)
        #Alanine
c13a<-gsub("GCT", "GCA", c12a, perl=TRUE)
c14a<-gsub("GCC", "GCT", c13a, perl=TRUE)
c15a<-gsub("GCG", "GCC", c14a, perl=TRUE)
        #Asparagine
c16a<-gsub("AAT", "AAC", c15a, perl=TRUE)
        #Leucine
c17a<-gsub("TTG", "CTT", c16a, perl=TRUE)
c18a<-gsub("CTA", "TTG", c17a, perl=TRUE)
c19a<-gsub("CTG", "CTA", c18a, perl=TRUE)
c20a<-gsub("CTC", "CTG", c19a, perl=TRUE)
c21a<-gsub("TTA", "CTC", c20a, perl=TRUE)
        #Glycine
c22a<-gsub("GGA", "GGT", c21a, perl=TRUE)
c23a<-gsub("GGG", "GGA", c22a, perl=TRUE)
c24a<-gsub("GGC", "GGG", c23a, perl=TRUE)
        #Tyrosine
c25a<-gsub("TAT", "TAC", c24a, perl=TRUE)
        #Cysteine
c26a<-gsub("TGC", "TGT", c25a, perl=TRUE)
        #Serine
```

```
c27a<-gsub("AGC", "TCG", c26a, perl=TRUE)
c28a<-gsub("AGT", "AGC", c27a, perl=TRUE)
c29a<-gsub("TCC", "AGT", c28a, perl=TRUE)
c30a<-gsub("TCT", "TCC", c29a, perl=TRUE)
c31a<-gsub("TCA", "TCT", c30a, perl=TRUE)
        #Threonine
c32a<-gsub("ACT", "ACA", c31a, perl=TRUE)
c33a<-gsub("ACC", "ACT", c32a, perl=TRUE)
c34a<-gsub("ACG", "ACC", c33a, perl=TRUE)
        #Proline
c35a<-gsub("CCT", "CCA", c34a, perl=TRUE)
c36a<-gsub("CCC", "CCT", c35a, perl=TRUE)
c37a<-gsub("CCG", "CCC", c36a, perl=TRUE)
        #Aspartate
c38a<-gsub("GAT", "GAC", c37a, perl=TRUE)
        #Glutamate
c39a<-gsub("GAA", "GAG", c38a, perl=TRUE)
        #Phenylalanine
c40a<-gsub("TTC", "TTT", c39a, perl=TRUE)
        #Lysine
c41a<-gsub("AAG", "AAA", c40a, perl=TRUE)

#Switch 1
        #Valine
c0b<-gsub("GTA", "GTC", c41a, perl=TRUE)
c1b<-gsub("GTG", "GTT", c0b, perl=TRUE)
        #Histidine
c2b<-gsub("CAT", "CAC", c1b, perl=TRUE)
        #Glutamine
c3b<-gsub("CAA", "CAG", c2b, perl=TRUE)
        #Arginine
c4b<-gsub("CGG", "CGA", c3b, perl=TRUE)
        #Isoleucine
c5b<-gsub("ATA", "ATT", c4b, perl=TRUE)
        #Alanine
c6b<-gsub("GCA", "GCG", c5b, perl=TRUE)
        #Asparagine
c7b<-gsub("AAC", "AAT", c6b, perl=TRUE)
        #Leucine
c8b<-gsub("CTT", "TTA", c7b, perl=TRUE)
        #Glycine
c9b<-gsub("GGT", "GGC", c8b, perl=TRUE)
        #Tyrosine
c10b<-gsub("TAC", "TAT", c9b, perl=TRUE)
        #Cysteine
c11b<-gsub("TGT", "TGC", c10b, perl=TRUE)
        #Serine
c12b<-gsub("TCG", "TCA", c11b, perl=TRUE)
        #Threonine
c13b<-gsub("ACA", "ACG", c12b, perl=TRUE)
        #Proline
c14b<-gsub("CCA", "CCG", c13b, perl=TRUE)
        #Aspartate
c15b<-gsub("GAC", "GAT", c14b, perl=TRUE)
        #Glutamate
c16b<-gsub("GAG", "GAA", c15b, perl=TRUE)
        #Phenylalanine
c17b<-gsub("TTT", "TTC", c16b, perl=TRUE)
        #Lysine
c18b<-gsub("AAA", "AAG", c17b, perl=TRUE)
```

```
#Shuffle 2
        #Valine
c1c<-gsub("GTA", "GTG", c41a, perl=TRUE)
c2c<-gsub("GTC", "GTA", c1c, perl=TRUE)
c3c<-gsub("GTT", "GTC", c2c, perl=TRUE)
        #Histidine
c4c<-gsub("CAC", "CAT", c3c, perl=TRUE)
        #Glutamine
c5c<-gsub("CAG", "CAA", c4c, perl=TRUE)
        #Arginine
c6c<-gsub("AGA", "CGG", c5c, perl=TRUE)
c7c<-gsub("AGG", "AGA", c6c, perl=TRUE)
c8c<-gsub("CGT", "AGG", c7c, perl=TRUE)
c9c<-gsub("CGC", "CGT", c8c, perl=TRUE)
c10c<-gsub("CGA", "CGC", c9c, perl=TRUE)
        #Isoleucine
c11c<-gsub("ATC", "ATA", c10c, perl=TRUE)
c12c<-gsub("ATT", "ATC", c11c, perl=TRUE)
        #Alanine
c13c<-gsub("GCT", "GCA", c12c, perl=TRUE)
c14c<-gsub("GCC", "GCT", c13c, perl=TRUE)
c15c<-gsub("GCG", "GCC", c14c, perl=TRUE)
        #Asparagine
c16c<-gsub("AAT", "AAC", c15c, perl=TRUE)
        #Leucine
c17c<-gsub("TTG", "CTT", c16c, perl=TRUE)
c18c<-gsub("CTA", "TTG", c17c, perl=TRUE)
c19c<-gsub("CTG", "CTA", c18c, perl=TRUE)
c20c<-gsub("CTC", "CTG", c19c, perl=TRUE)
c21c<-gsub("TTA", "CTC", c20c, perl=TRUE)
        #Glycine
c22c<-gsub("GGA", "GGT", c21c, perl=TRUE)
c23c<-gsub("GGG", "GGA", c22c, perl=TRUE)
c24c<-gsub("GGC", "GGG", c23c, perl=TRUE)
        #Tyrosine
c25c<-gsub("TAT", "TAC", c24c, perl=TRUE)
        #Cysteine
c26c<-gsub("TGC", "TGT", c25c, perl=TRUE)
        #Serine
c27c<-gsub("AGC", "TCG", c26c, perl=TRUE)
c28c<-gsub("AGT", "AGC", c27c, perl=TRUE)
c29c<-gsub("TCC", "AGT", c28c, perl=TRUE)
c30c<-gsub("TCT", "TCC", c29c, perl=TRUE)
c31c<-gsub("TCA", "TCT", c30c, perl=TRUE)
        #Threonine
c32c<-gsub("ACT", "ACA", c31c, perl=TRUE)
c33c<-gsub("ACC", "ACT", c32c, perl=TRUE)
c34c<-gsub("ACG", "ACC", c33c, perl=TRUE)
        #Proline
c35c<-gsub("CCT", "CCA", c34c, perl=TRUE)
c36c<-gsub("CCC", "CCT", c35c, perl=TRUE)
c37c<-gsub("CCG", "CCC", c36c, perl=TRUE)
        #Aspartate
c38c<-gsub("GAT", "GAC", c37c, perl=TRUE)
        #Glutamate
c39c<-gsub("GAA", "GAG", c38c, perl=TRUE)
        #Phenylalanine
c40c<-gsub("TTC", "TTT", c39c, perl=TRUE)
        #Lysine
c41c<-gsub("AAG", "AAA", c40c, perl=TRUE)
```

```
#Switch 2
        #Valine
c0d<-gsub("GTA", "GTC", c41c, perl=TRUE)
c1d<-gsub("GTG", "GTT", c0d, perl=TRUE)
        #Histidine
c2d<-gsub("CAT", "CAC", c1d, perl=TRUE)
        #Glutamine
c3d<-gsub("CAA", "CAG", c2d, perl=TRUE)
        #Arginine
c4d<-gsub("CGG", "CGA", c3d, perl=TRUE)
        #Isoleucine
c5d<-gsub("ATA", "ATT", c4d, perl=TRUE)
        #Alanine
c6d<-gsub("GCA", "GCG", c5d, perl=TRUE)
        #Asparagine
c7d<-gsub("AAC", "AAT", c6d, perl=TRUE)
        #Leucine
c8d<-gsub("CTT", "TTA", c7d, perl=TRUE)
        #Glycine
c9d<-gsub("GGT", "GGC", c8d, perl=TRUE)
        #Tyrosine
c10d<-gsub("TAC", "TAT", c9d, perl=TRUE)
        #Cysteine
c11d<-gsub("TGT", "TGC", c10d, perl=TRUE)
        #Serine
c12d<-gsub("TCG", "TCA", c11d, perl=TRUE)
        #Threonine
c13d<-gsub("ACA", "ACG", c12d, perl=TRUE)
        #Proline
c14d<-gsub("CCA", "CCG", c13d, perl=TRUE)
        #Aspartate
c15d<-gsub("GAC", "GAT", c14d, perl=TRUE)
        #Glutamate
c16d<-gsub("GAG", "GAA", c15d, perl=TRUE)
        #Phenylalanine
c17d<-gsub("TTT", "TTC", c16d, perl=TRUE)
        #Lysine
c18d<-gsub("AAA", "AAG", c17d, perl=TRUE)

Code1<-c41a
Code2<-c18b
Code3<-c41c
Code4<-c18d

Code1
Code2
Code3
Code4
```

The published article includes all code generated or analyzed during this study and did not generate any datasets.